Organic Metals and Superconductors Based on BETS (BETS = Bis(ethylenedithio)tetraselenafulvalene)

Hayao Kobayashi* and HengBo Cui

Institute for Molecular Science and CREST, Okazaki 444-8585, Japan

Akiko Kobayashi

Research Center for Spectrochemistry, Graduate School of Science, The University of Tokyo, Hongo, Bunkyo-ku, Tokyo 113-0033, Japan

Received March 9, 2004

Contents

1. Introduction

1.1. Brief History of Development of Organic Metals and Magnetic Organic Conductors

Since the discovery of the first organic superconductors $(TMTSF)_2X$ (TMTSF = tetramethyltetraselenafulvalene (see Figure 1); X = PF_6, ClO_4, ...) about a quarter century ago,[1] extremely large progress has been achieved in the field of physics and chemistry of molecular conductors. Contrary to the physicists interested in the unified interpretation on the common nature of various conductors, chemists are usually interested in the individuality of each molecular conductor. Consequently, for most of the chemists in this field, the largest concern has been the development of a new type of molecular conductors. When the metallic states of TMTSF conductors were found to be stable down to about 10 K,[2] many chemists noticed the possibility of the existence of two-dimensional (2-D) organic conductors with intermolecular 2-D networks of peripheral chalcogen atoms of π molecules,[3] although all the molecular metals developed in the 1970s were believed to be 1-D systems because face-to-face stacking of planar π molecules had been believed to be essential to construct the π conduction band. Thus, the discovery of Bechgaard salts pushed us to evaluate the dimensionality of the organic conductor. To take a step forward, we adopted a simple extended Hückel tight-binding band calculation at that time, which provided a very useful tool to treat semiquantitatively the molecular design of organic conductors. From the viewpoint of molecular design, the extended-Hückel tight-binding band calculation can be regarded as a transformation of the anisotropy of intermolecular interactions in real space into the anisotropy of the system in the momentum space. By adopting the extended Hückel approximation ($t \propto S$), both anisotropy of intermolecular short contacts and anisotropy of frontier molecular orbitals forming the conduction band are included simultaneously, where t and S are the transfer integral and the intermolecular overlap integral of the frontier orbitals, respectively. Despite of the close 2-D molecular arrangement, the tight-binding band calculation suggested that $TMTSF_2X$ was an essentially 1-D system owing to the anisotropy of the π frontier orbitals.[4] Nevertheless, as expected, the extended Hückel tight-binding band examinations of a series of molecular conductors with the networks of peripheral chalcogen atoms gave us an important hint to develop new organic metals with stable 2-D cylindrical Fermi surfaces on the basis of multi-chalcogen π donor molecules. Then, by the observations of Shubnikov–de Haas (SdH) and de Haas–van Alphen (dHvA) oscillations in the subsequently developed BEDT-TTF (=bis(ethylenedithio)-tetrathiafulvalene) superconductors with β and κ type

* Corresponding author. Tel: +81-564-55-7410. Fax: +81-564-54-2254. E-mail: hayao@ims.ac.jp.

10.1021/cr030657d CCC: $48.50
Published on Web 08/18/2004

Hayao Kobayashi was born in 1942 in Tokyo, Japan. He studied chemistry at the University of Tokyo. He received his M.S. (1967) and Ph.D. (1970) degrees from the University of Tokyo. He became Lecturer at Toho University in 1971 and was promoted to Professor in 1980. He moved in 1995 to the Institute for Molecular Science in Okazaki. He started his research on molecular conductors when he became a doctoral student in 1967. Since then, he has studied various molecular conductors, such as TCNQ complexes, partially oxidized 1-D platinum complexes, BEDT-TTF, $M(dmit)_2$, DCNQI, and BETS systems, and recently single-component molecular metals. His present main interests are in the design and development of multifunctional molecular systems including porous materials with novel electronic functions.

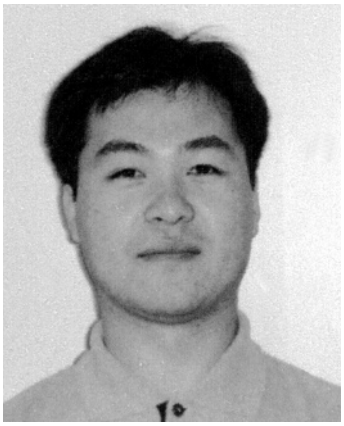

HengBo Cui was born in Jilin Province, China, in 1971. He received his master's degree from YanBian University, China, in 1996. He the became a research associate at College of Pharmacy, YanBian University, China. He obtained his Ph.D. degree from the University of Tokyo, Japan, in 2003 with studies on organic metals with magnetic lanthanoid anions. His present research interests are in the physical properties of functional molecular systems such as magnetic molecular metals, superconductors, and porous molecular systems.

molecular arrangements,[5−7] the existence of ideally 2-D organic π metal systems with stable metallic states was finally accepted. Through these works, the old image of organic metal was renewed. It became known that the molecular metals were regarded as the clean systems with well-defined Fermi surfaces. Almost at the same time, the molecular superconductors based on multi-chalcogen π acceptor molecules $M(dmit)_2$ (M = Ni, Pd) (see Figure 1) were also discovered.[8] Thus, the first stage of the development of new molecular metals and superconductors based on multi-sulfur (or selenium) π molecules had been almost accomplished until the beginning of 1990s. And the π conduction electrons, which had been confined within 1-D systems until the discovery of Bechgaard salts, have freedom in 2-D spaces. However, in the midst of this rapid progress, an extraordinarily large impact was brought about by the discovery of high-temperature cupper oxide superconductors.[9] It became very serious for the chemists in this field to find new ways by making the best use of the merit of molecule-based systems.

Akiko Kobayashi was born in 1943 in Tokyo, Japan. She studied chemistry at the University of Tokyo and obtained a Ph.D. in 1972. She became a research associate at the University of Tokyo in 1972 and was promoted to an Associate Professor at the Department of Chemistry in 1993. In 1999, she took a position as a Professor at the Research Centre for Spectrochemistry, Graduate School of Science, University of Tokyo. She studied molecular conductors, such as 1-D platinum complexes, BEDT-TTF, $M(dmit)_2$, DCNQI, and BETS systems, and recently single-component molecular metals. Her present research interests are in the development of various types of molecular systems with novel physical properties.

Around the same time, a new type of organic conductor $(DMe\text{-}DCNQI)_2Cu$ with a stable metallic state down to very low temperature was reported by Aumüller et al. (DMe-DCNQI = 2,5-dimethyldicyanoquinodiimine (Figure 1)).[10] Considering that all the organic conductors based on TCNQ cannot retain the metallic state down to low temperature, it was very curious for the conductor consisting of a similar simple π acceptor molecule without sufficiently large intermolecular transverse interactions to have a stable metallic state even at liquid helium temperature. However, it was soon pointed out that the Cu atom connecting 1-D columns of π acceptor molecules (DMe-DCNQI) is in a mixed-valence state ($Cu^{+1.3}$).[11,12] Because of the mixed valency of Cu, the highest occupied 3d orbital of Cu was considered to take part in the formation of conduction band.[11] Therefore, the unique $\pi-d$ hybridized metal band is realized when the system is in a metallic state. The existence of $\pi-d$ hybrid band was confirmed by low-temperature magnetoresistance experiments and the first principle band structure calculation based on the local density approximation (LDA).[13,14] In the analogous system $(R_1,R_2\text{-}DCNQI)_2Cu$ (R_1, R_2 = Me, Br; Br, Br; Me, Cl; or Cl, Cl) exhibiting a metal−insulator transition coupled with Jahn−Teller-like distortion of coordination structure around Cu, the localized magnetic moments of Cu^{2+} appear below T_{MI}, which were found to be antiferomagnetically ordered at low temperatures.[15] Alhough the interplay between localized magnetic moments and π metal electrons could not be realized in these systems due to the appearance of localized 3d moments only in the insulating states, $(R_1,R_2\text{-}DCNQI)_2Cu$ stimulated us in developing new molecular conductors where the $\pi-d$ interaction plays a crucial role.

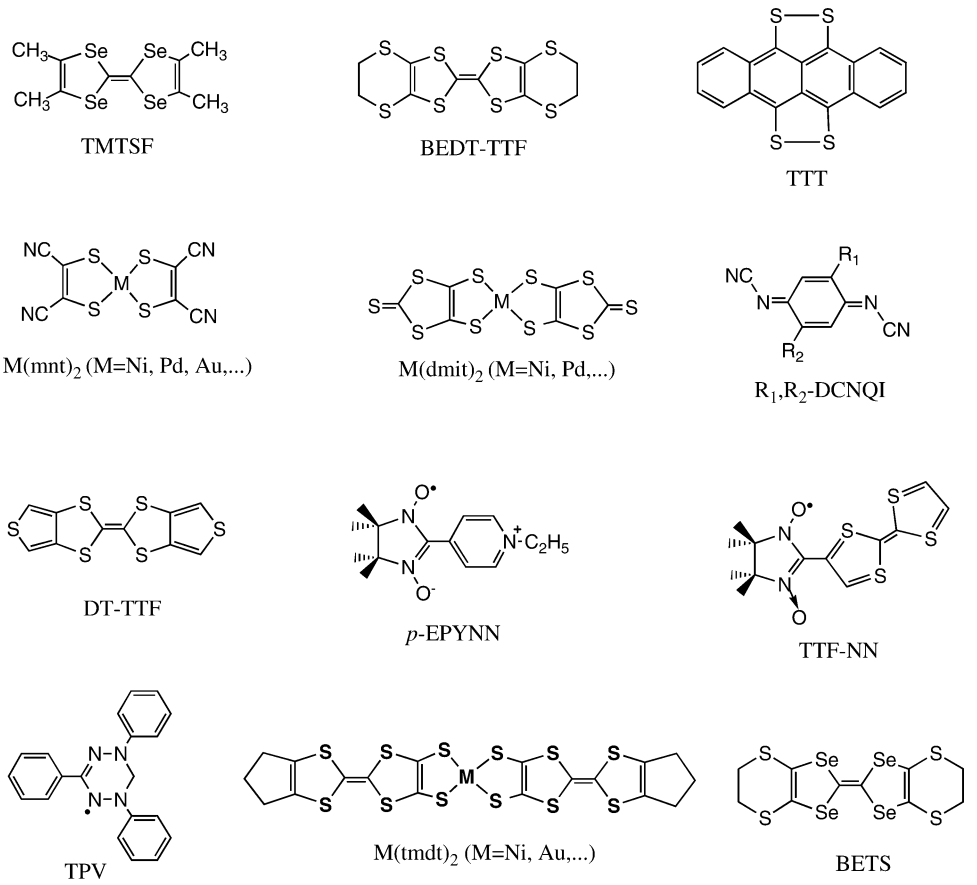

Figure 1. Molecules and abbreviations.

Phthalocyanine (Pc) complexes have long attracted large interest as possible candidates of magnetic molecular conductors. It is well-known that the paramagnetic ions such as Co^{2+} and Cu^{2+} are incorporated in Pc conductors, where the paramagnetic ions form a linear magnetic chain embedded within 1-D Fermi sea of organic carriers and are strongly coupled to π conduction electrons.[16] Recently, not only planar Pc molecules but also an axially substituted Pc complex carrying magnetic center such as TPP-$[Fe^{III}(PC)(CN)_2]_2$ (TPP = tetraphenylphosphonium) were reported.[17] Compared with isostructural nonmagnetic weakly semiconducting Co^{III} salt with the activation energy less than 0.01 eV, the resistivity of Fe^{III} salt is much larger especially at low temperature. But the Fe^{III} salt shows an isotropic large negative magnetoresistance. Coupled 1-D electronic and magnetic properties have been reported also in (perylene)$_2$[M(mnt)$_2$] complexes (M = Ni, Pd, Pt, Fe, ...; mnt^{2-} = maleonitriledithiolate (see Figure 1)).[18] In (perylene)$_2$[Ni(mnt)$_2$], for example, a large paramagnetic susceptibility is due to the large paramagnetic contribution from the Ni(mnt)$_2$ component in addition to the Pauli susceptibility from π conduction electrons in the perylene chains. At 25 K, Peierls and spin-Peierls transitions simultaneously take place in the conduction (perylene) and magnetic (Ni(mnt)$_2$) chains, respectively, but the existence of a real interplay is not yet established. Recently, Ribera et al. have found a spin-ladder complex based on π donor molecule DT-TTF and diamagnetic Au(mnt)$_2$ (DT-TTF = dithionephenotetrathiafulvalene (Figure 1).[19] Unlike highly conducting isostructural Ni(mnt)$_2$ and Pd(mnt)$_2$ conductors exhibiting metal-like behavior and insulator transitions around 120 K, (DT-TTF)$_2$Au(mnt)$_2$ is less conducting and behaves as a semiconductor even at room temperature. However, the magnetic susceptibility was found to be able to be fitted to a two-legged spin-ladder model. Spin-ladder behavior has been also reported in the Ni(dmit)$_2$ complex, *p*-EPYNN[Ni(dmit)$_2$] (*p*-EPYNN = *p*-*N*-ethylpyridinium α-nitronyl nitoxide), where $[Ni(dmit)_2]^-$ plays an important role in the formation of an antiferromagnetic molecular spin ladder.[20] It is expected that the nonhalf filling spin-ladder system can exhibit superconducting behavior.[21] But this system is of course an insulator, and the interplay of π conduction electrons and magnetism cannot be expected.

The design of organic conductors with the coexistence of organic radical spins and π metal electrons has been one of the long-standing targets in the development of new organic conductors. However, it seems fairly difficult for the conductors based on the organic molecules such as *p*-EPYNN, TTF-NN, and TPV containing stable radical parts such as nitronyl nitroxyde and verdazyl radical (see Figure 1) to construct the molecular arrangements suitable for the formation of π metal bands.[22,23] In fact, all the complexes ever obtained were found to be insulators. The minimal requirements for the design of the molecular metals are the formation of conduction bands and generation of charge carriers.[24,25] But the formation of molecular arrangement suitable not only for the desirable intermolecular magnetic interaction but also for the formation of the π metal band is not

so easy. Very recently, we found that extended-TTF molecules with proxyl radicals are good building blocks to construct the molecular conductors where π metal electrons and organic radical spins coexist.[26]

Since the molecules tend to keep their independence even in the solid state, in the molecular material consisting of two kinds of building blocks, two functions originating from these two components with different characters will coexist. In Bechgaard-type salt (D_2X) consisting of π donor molecules (D) and inorganic anions (X), the anion plays an important role not only in the construction of crystal structure as a counterpart of donor molecule but also in the generation of charge carriers by extracting π electrons from the conduction band formed from the frontier orbitals of π donor molecules. However, until recently, the role of the anions such as PF_6^- and ClO_4^- has been regarded less important because the Fermi surfaces dominating the metallic character of the system are determined mainly by the donor arrangement. But if we can construct the Bechgaard type salt by using the magnetic anions, the system will show the multifunctional electromagnetic properties if there exists the considerable interaction between conduction part and magnetic part. In 1995, Kurmoo et al. found that the paramagnetic organic superconductors (BEDT-TTF)$_4$A$Fe(C_2O_4)_3C_6H_5CN$ (A = H_3O^+) exhibit a superconducting transition at 7 K.[27] The salt can be regarded as an example of organic/inorganic molecular composite or chemically constructed multilayer. The crystal structure consists of successive layers of BEDT-TTF and layers of approximately hexagonal geometry containing alternating H_3O^+ and $Fe(C_2O_4)_3^{3-}$, lying within the hexagonal cavities. However, the coupling between π conduction electrons and paramagnetic anion layers seems to be negligible, and any distinct dual-action phenomena of magnetism and (super)conductivity could not be observed. The isostructural salts with K^+ and NH_4^+ are semiconductors.

Coronado et al. have found the first ferromagnetic organic metal, BEDT-$TTF_3[MnCr(C_2O_4)_3]$, with "chemically constructed multilayer structure".[28] The system is a soft magnet with ferromagnetic transition temperature T_c of about 5.5 K and very small coercive field ($H_c \approx 5-10$ Oe). The magnetic properties are almost the same to those observed in molecular magnets $\{NBu_4[MCr(ox)_3]\}_x$ (NBu_4^+ = tetra(*n*-buthyl)ammonium).[29] Although the coexistence of metallic conductivity and ferromagnetic order was realized, the conduction layers and magnetic layers seem to be almost independent to each other. In addition to the BEDT-TTF compound, Coronado et al. have recently reported similar ferromagnetic organic metal with BETS conduction layers, $[BETS]_x[MnCr(ox)_3](CH_2Cl_2)$ ($x \approx 3$) (see Table 1 and the references therein), where BETS = bis(ethylenedithio)tetraselenafulvalene) is a modification of BEDT-TTF obtained by substituting selenium for sulfur in the central tetrathiafulvalene fragment (see Figure 1).

Recently, we have reported the first molecular metal consisting of single-component molecules, Ni(tmdt)$_2$, and analogous single-component molecular metals, Au(tmdt)$_2$, which is, to our best knowledge, the first molecular conductor exhibiting (antiferro)-magnetic transition at the temperature as high as about 100 K without loss of its high conductivity.[24,25,30]

Since the molecular materials are the systems whose properties are directly derived from the nature of the component molecules, the bulk properties of molecular systems—whether optical, magnetic or electrical—can be controlled in principle by the rational design of the nanosized functional units, that is, the molecule.[31] Magnetic organic conductors consisting of organic π donors and inorganic anions may be a good example. However, if we wish to obtain the molecular system with significant bifunctionality, the interaction between π metal electrons and localized magnetic moments must be sufficiently large.

More than a decade ago, we started to try to prepare magnetic organic conductors based on BETS molecules and tetrahalide Fe^{3+} ions.[32] At first, the interaction between the π conduction electrons and the localized 3d magnetic moments of anions was considered to be fairly weak because there is no direct overlap between the frontier π orbitals and the magnetic 3d orbitals. Therefore, it was considered that the stabilization of metallic state down to very low temperature is an essential requirement to observe the interplay of π metal electrons and localized magnetic moments. This was the reason we adopted the BETS molecule. Fortunately, the $\pi-$d interaction in BETS conductors was discovered to be not so weak, and we could obtain very unique magnetic organic superconductors besides conventional organic superconductors with nonmagnetic anions.

2. Synthesis and Electrical Properties of BETS Conductors

2.1. Synthesis and Electrocrystallization

Although the synthesis of BETS was first reported by Schmaker et al. more than two decades ago, the properties of BETS complexes remained elusive.[33] Kato et al. have developed a reliable titanocene-involving synthetic method using selenium powder as selenium sources (Scheme 1).[34] To avoid the use of malodorous benzylmercaptan, to reduce the number of reaction steps, and to increase yields, this procedure was further improved: a convenient one-step reaction for the preparation of 2,3-dihydro-1,4-dithiin was established.[35]

Very recently, Takimiya et al. have reported a general method for the synthesis of alkylenedithio- and bis(alkylenedithio)tetraselenafulvalenes including BETS.[36] They also presented a CSe_2-free synthesis of the key intermediate, 2,6(7′)-bis(methylthio)-3,7(6′)-bis(2-methoxycarbonylethylethylthio)tetraselenaful valene from parent tetraselenafulvalene (TSF).

The crystals of BETS salts with MX_4^{n-} anions (M = Ga, Fe, In, Co, Ni, Mn, ...) were prepared by electrochemical oxidation of BETS (about 6 mg) in an appropriate solvent (about 15 mL; 10% ethanole/chrolobenzene, chrolobenzene, 1,1,2-trichloroethane, tetrahydrofuran, ...), with the corresponding tetra-

Table 1. Structural and Electrical Properties of BETS Compounds

	Compound	structure type	space group	*a* (Å)	*b* (Å)	*c* (Å)	α (deg)	*β*	*γ*	electrical property	ref
1	BETS[a]		$P2_1/c$	6.662	14.227	16.216		92.97			34, 35
2	$(BETS)_2PF_6(TCE)_x$	κ	$C2/c$	38.022	8.387	12.005		91.45		M[h] down to 4 K	34
3	$(BETS)_2AsF_6(TCE)_x$	κ	$C2/c$	38.219	8.406	12.052		90.04		M down to 4 K	34
4	$(BETS)_2SbF_6$	κ	$C2/c$	35.310	8.434	11.511		99.45		M down to 4 K	34
5	$(BETS)_2TaF_6$	κ	$C2/c$	35.163	8.362	11.636		99.44		M down to 4 K	34b
6	$(BETS)_2TaF_6$	θ	$C2/c$	37.97	4.240	11.596		100.21		M down to 50 K	34
7	$(BETS)_2ClO_4(TCE)_x$	$\kappa(4\times4)$[b]	$P2_1/c$	19.253	8.568	22.551		109.06		M down to 4 K	38
8	$(BETS)_2BF_4(TCE)_x$	$\kappa(4\times4)$	$P2_1/c$	19.122	8.559	22.568		109.23		M down to 4 K	38
9	$(BETS)_4HgBr_4(PhCl)_x$	θ	$I4_1/a$	9.742		75.68				M down to 4 K	38, 39
10	$(BETS)HgBr_x$	κ	$P2_1/c$	39.064	8.654	11.516		106.13		M down to 4 K	34, 38
11	$(BETS)_2I_3$	α	$P\bar{1}$	9.209	10.816	17.777	96.63	97.87	90.69	M−I T_{MI} = 50 K	34
12	$(BETS)_2IBr_2$	α	$P\bar{1}$	9.209	10.820	17.758	96.69	97.92	90.64	M−I T_{MI} = 45 K	34
13	$(BETS)_2AuI_2$	α	$P\bar{1}$	9.197	10.808	17.713	96.90	97.84	90.65	M−I T_{MI} = 45 K	34
14	$(BETS)_2ICl_2$		$P\bar{1}$	16.619	12.311	8.854	113.06	92.0	93.34	M−I T_{MI} = 110 K	34
15	$(BETS)_2GaCl_4$	λ	$P\bar{1}$	16.172	18.616	6.607	98.38	96.75	112.56	SC T_c = 5.5 K	32, 58
16	$(BETS)_2FeCl_4$	λ	$P\bar{1}$	16.164	18.538	6.593	98.40	96.67	112.52	M−I $T_N(=T_{MI})$ = 8.3 K[c]	32, 59
17	$(BETS)_2GaCl_4$	κ	Pnma	11.665	35.894	8.464				M down to 2 K	32
18	$(BETS)_2GaBr_4$	κ	Pnma	11.773	36.635	8.492				SC T_c = 1 K	32
19	$(BETS)_2FeCl_4$	κ	Pnma	11.693	35.945	8.491				T_N, T_c = 0.5, 0.2 K[d]	32
20	$(BETS)_2FeBr_4$	κ	Pnma	11.787	36.607	8.504				T_N, T_c = 2.5, 1.1 K[e]	32
21	$(BETS)_2TlCl_4$	κ	Pnma	11.611	36.59	8.557				SC T_c = 2.5 K	40
22	$(BETS)_2InCl_4$	κ	Pnma	11.586	36.492	8.536				M down to 4 K	32
23	$(BETS)_2GaBr_4$	λ′	$P\bar{1}$	16.360	17.329	6.638	91.80	98.90	94.53	high cond.−I at 50 K	59
24	$(BETS)_2Cu[N(CN)_2]B$ r	κ	Pnma	12.961	31.005	8.576				M down to 4 K	41
25	$(BETS)_2CF_3SO_3$	κ	$P2_1/a$	11.732	8.332	34.972		99.68		M down to 50 K	41
26	$(BETS)_2Tl\ I_4$		$C2/c$	11.902	41.067	8.532		110.13		semiconductor	42
27	$(BETS)_2TlI_4(I_3)$	κ	Pcab	15.267	16.213	36.131				semiconductor	42
28	$(BETS)_4Hg_3I_8$	κ	$P2_1/a$	16.783	21.408	11.744	101.99	109.38	75.87	M down to 200 K	42
29	$(BETS)_2KHg(SCN)_4$	α	$P\bar{1}$	10.069	20.925	9.968	103.37	90.28	93.30	M down to 0.4 K	42
30	$(BETS)_2NH_4Hg(SCN)_4$	α	$P\bar{1}$	10.125	20.940	9.981	103.46	90.37	93.18	M down to 0.4 K	42
31	$(BETS)_2C(CN)_3$	κ	$A2/a$	11.583	35.086	8.532		91.10		M down to 1.3 K	43
32	$(BETS)_4[Fe(CN)_5NO]$	θ	$C2/c$	40.259	4.177	11.599		97.23		M down to 40 K	44
33	$(BETS)_2[FeBr_5NO]$	θ	$C2/c$	7.480	41.065	12.514		105.00		semiconductor	45
34	$(BETS)_4[RuCl_5NO]$		$P\bar{1}$	8.858	10.367	11.351	110.52	97.46	105.46	semiconductor	45
35	$(BETS)_4CoCl_4(ETOH)$	κ	Pccn	8.458	35.638	11.817				M down to 2 K	46
36	$(BETS)_2CoCl_4$		$P\bar{1}$	12.477	16.907	8.920	93.30	109.19	79.65	semiconductor	46
37	$(BETS)_4MnBr_4\ (EtOH)_2$	θ	$I4_1/a$	9.771		75.783				M down to 30 K	46
38	$(BETS)_4Cl[C_2H_5(OH)_2]$	κ	$C2/c$	34.995	8.505	11.878		106.78		M down to 4 K	47
39	$(BETS)_4Br[C_2H_5(OH)_2]$	κ	$C2/c$	35.367	8.507	11.974		106.92		M down to 1K	47
40	$(BETS)_4Cu_2Cl_6$	θ	Pbcn	9.543	34.897	20.043				M down to 4 K	48
41	$(BETS)_2Cu_5I_6$	α	$P2_1$	11.629	4.246	21.853		100.09		M down to 25 K	49
42	$(BETS)_5Te_2I_6$		$P2_1/n$	21.637	10.760	21.001		115.72		weakly metallic	34c
43	$(BETS)_6Bi_3Cl_{12}(PhCl)$	α	$P\bar{1}$	19.46	11.280	14.98	67.32	85.55	82.29	M down to 200 K	50
44	$(BETS)_6Bi_2Cl_8$		$P2_1/n$	24.67	22.73	7.508		98.56		semiconductor	50
45	$(BETS)_2TlHg(SeCN)_4$	α	$P\bar{1}$	10.149	21.187	10.081	103.41	90.45	93.22	M down to 1.5 K	51
46	$(BETS)_2InCl_5[(C_2H_5)_4N]_{0.7}$		$P2_1/a$	20.469	9.670	23.444		96.64		M down to 50 K	52
47	$(BETS)_2[Pd(dts)_2]_2$		$P2_1/c$	8.512	27.849	8.938		108.69		semiconductor	53
48	$(BETS)_2[Pd(dts)_2]_2(T\ CE)_2$		$P2_1/c$	17.954	13.468	10.896		90.11		semiconductor	53
49	$(BETS)_5[Pd(dts)_2]_2$		$P2_1/c$	11.952	4.159	18.708		106.24		M down to 4 K	53
50	$(BETS)[Au(dts)_2]$		$P\bar{1}$	8.036	14.112	5.886	91.99	97.00	104.79	semiconductor	53
51	$(BETS)_x[MnCr(C_2O_4)_2]$[f]		$P\bar{1}$	4.356	11.575	20.090	91.71	92.90	90.04	M down to 150 K	54
52	$(BETS)_2InBr_4$	κ	Pnma	11.676	37.509	8.581				M down to 4 K	55
53	$(BETS)TlCl_5$		$P\bar{1}$	9.052	10.542	6.210	103.56	100.76	67.07	semiconductor	55
54	$(BETS)TlBr_5$		$P\bar{1}$	8.709	11.333	12.069	93.80	103.02	93.40		55
55	$(BETS)_2TlBr_4$	λ″	$P\bar{1}$	6.643	18.577	31.27	81.45	87.11	80.24	semiconductor	55
56	$(BETS)_2InI_4$	α	$C2/c$	11.802	40.984	8.484		110.09		semiconductor	55
57	$(BETS)_2Cl(COOH)_2$	κ	$C2/c$	35.534	11.405	8.393		92.17		M down to 1 K	55
58	$(BETS)_3InCl_5(PhCl)_{0.5}$		$P2_1/n$	21.812	10.352	24.964		104.83		M down to 50K	55
59	$(BETS)GaBr_4$		$P\bar{1}$	7.050	8.489	24.142	85.63	83.79	68.85	M down to 20 K	55
60	$(BETS)FeBr_4$		$P\bar{1}$	8.642	11.238	11.197	93.90	103.24	93.31	semiconductor, T_N = 2 K	55
61	$(BETS)_2(Cl_2TCNQ)$	D_2A	$P\bar{1}$	13.176	18.896	4.193	93.69	92.71	101.98	SC T_c = 1.3 K[g]	56
62	$(BETS)_2(Br_2TCNQ)$	D_2A	$P\bar{1}$	13.174	19.041	4.210	94.27	93.69	101.69	M down to 13 K	56, 60

[a] Isomorphous to ET. [b] Conduction plane is constructed of two types of BETS tetramers whose stacking directions are orthogonal to each other. [c] Antiferromagnetic and metal−insulator transitions take place cooperatively. The system exhibits a field-induced metal phase above 11 T and field-induced superconducting state around 33 T. [d] The second antiferromagnetic superconductor. [e] The first antiferromagnetic superconductor. The field-induced superconducting state appears around 12.5 T. [f] The crystal contain crystal solvent (CH_2Cl_2) and $x \approx 3$. [g] The first organic superconductor consisting of organic donor and acceptor columns. [h] M = metal; SC = superconductor; AFSC = antiferromagnetic superconductor; M−I = metal-to-insulator transition. TCE = 1,1,2-trichloroethane; PhCl = chlorobenzene; dts = dithiosquarato.

ethlyammonium salt of MX_4^{n-} (about 50 mg). H-Shaped glass tube cells without a glass frit and platinum wire electrodes with 1 mm diameter were used. Usually constant current (0.3−0.8 μA) was applied for 10−15 days. For example, the preparation condition of the single crystals of κ-$(BETS)_2FeBr_4$ usually adopted by us was as follows: BETS (6.5 mg) and tetraethylammonium iron(III) tetrabromide (57.2

Scheme 1

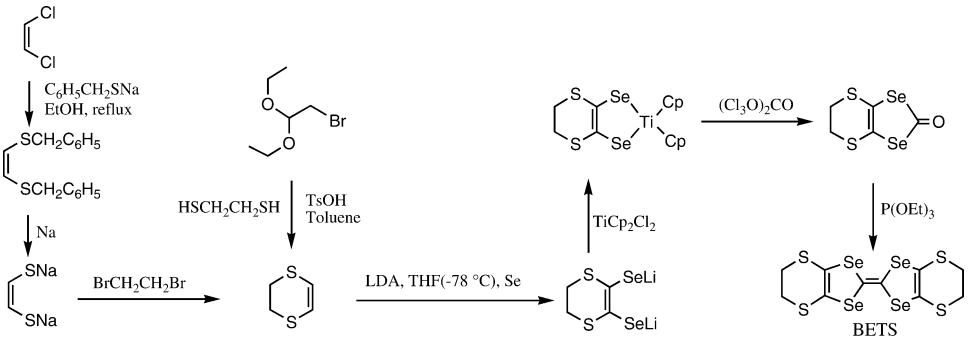

mg) are dissolved in 10% ethanol/chlorobenzene solution (15.0 mL) under nitrogen. A constant current (0.7 μA) is applied between the electrodes at room temperature or at 40 °C for 2−4 weeks. Thin plate-shaped crystals of κ-type structure are obtained.

As mentioned later in the paper, in the studies on BETS superconductors, the preparation of the crystals of mixed anion systems such as λ-,κ-(BETS)$_2$MBr$_x$Cl$_{4-x}$ (M = Fe, Ga) and λ-(BETS)$_2$Fe$_x$Ga$_{1-x}$Cl$_4$ is very important, where λ and κ are two main modifications of the crystals of BETS conductors. In the preparation of λ-(BETS)$_2$GaBr$_x$Cl$_{4-x}$, the mixed electrolyte (Et$_4$N)GaCl$_4$ and (Et$_4$N)GaBr$_4$ with appropriate ratio (x) is used instead of (Et$_4$N)GaBr$_x$Cl$_{4-x}$ because the halogen exchange occurs and the equilibrium amount of GaBr$_n$Cl$_{4-n}^-$ (n = 0, 1, 2, 3, 4) coexist in the solution. Therefore, usually the electrocrystallization was started after allowing the mixed electrolyte solution to stand for 24 h. Since these five species (n = 0, 1, 2, 3, 4) are considered to be involved in the crystals, GaBr$_x$Cl$_{4-x}^-$ must be regarded as the average stoichiometry of these five tetrahalogenogallate ions.[37] This may be one of the reasons why the high-quality mixed-anion crystals can be prepared in these BETS conductors. Roughly speaking, when the mixing ratio of two ammonium anions is approximately 1:1, the average stoichiometry of anions in the crystal is nearly equal to the mixing ratio of the anions in the electrolyte. But for $x \approx 0.0$ or ≈ 1.0, the ratio deviates from the ideal line of $x = x_s$, where x_s is the ratio of MBr$_4^-$/MCl$_4^-$ (M = Fe, Ga) in the solution (Figure 2). The minor component tends to be included selectively. Similar x versus x_s relation was also observed in the electrocrystallization of λ-(BETS)$_2$Fe$_x$Ga$_{1-x}$Cl$_4$.

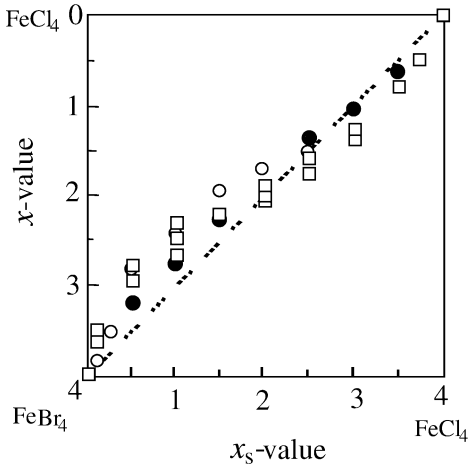

Figure 2. Relation between x-value of the crystal of κ-(BETS)$_2$FeBr$_x$Cl$_{4-x}$ and the mixing ratio of [(C$_2$H$_5$)$_4$N]FeBr$_4$ and [(C$_2$H$_5$)$_4$N]FeCl$_4$ in the solution of the electrocrystallization (x_s). The x-value was estimated from (1) the electron probe microanalysis (EPMA): open squares, (2) the X-ray population refinement of halogen atoms: filled circles, and (3) the empirical relation between unit cell volume and x [V (Å^3) = 3557 + 28x]: open circles.

2.2. Crystal Structures

The most advantageous feature of TTF-type π donor molecules in the design of the organic conductors is in the fact that HOMO (highest occupied molecular orbital) from which the conduction band is formed has a large amplitude and the same sign on every chalcogen atom. Because of the large electron cloud of the S (or Se) atom, intermolecular HOMO−HOMO overlap becomes large. Furthermore, because of the same sign of HOMO on every S (or Se) atom, every intermolecular S···S contact can contribute additively to enhance the intermolecular interaction (especially transverse interaction). This is not always true for other multi-sulfur π donor molecules. For example, the HOMO of another type multi-sulfur π donor molecule tetrationaphthalene (or tetrathiotetracene) has a nodal plane on the S−S bonds, which strongly reduces the transverse intermolecular HOMO−HOMO interaction.[25] This is the main reason multi-sulfur π molecules with a TTF-like structure have played a central role in the development of molecular conductors with stable 2-D metal bands. When we started to examine the BETS conductors around 1990, we expected that many stable molecular metals would be obtained because BETS will have large intermolecular transverse interactions due to the large Se atom in the central TTF skeleton. In fact, the first survey on BETS conductors with octahedral (PF$_6^-$, SbF$_6^-$, ...), tetrahedral (ClO$_4^-$, BF$_4^-$, ...), and linear (I$_3^-$, IBr$_2^-$, ...) anions revealed the strong tendency of the BETS molecule to form a stable metallic band.[34] Then by utilizing this properties of the BETS molecule, we tried to develop the organic metals where π metal electrons can interact with localized 3d magnetic moments of magnetic anions FeX$_4^-$ (X = Cl, Br) at a low temperature and also isostructural conductors with similar nonmagnetic tetrahalide anions MX$_4^-$ (M = Ga, In, ...).[32] To our knowledge, besides the alloy systems, there are approximately 60 BETS conductors whose crystal structures have been determined so far (see Table 1).

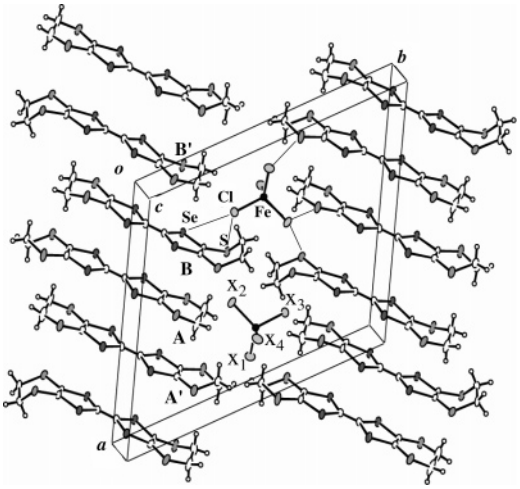

Figure 3. Crystal structure of λ-$(BETS)_2MCl_4$ (M = Fe, Ga). A and B are two independent BETS molecules, and X_1, X_2, X_3, and X_4 are four sites of halogen atoms. The short Cl···S (or Se) distances in λ-$(BETS)_2FeCl_4$ are shown by thin lines: Cl···Se = 3.528 Å and Cl···S = 3.417, 3.642, 3.648, and 3.674 Å.

From the salts with tetrahedral anions, several superconductors have been discovered except alloyed superconductors such as λ-$(BETS)_2Fe_xGa_{1-x}Cl_4$, λ-$(BETS)_2GaBr_xCl_{4-x}$, λ-$(BETS)_2Fe_xGa_{1-x}Br_yCl_{4-y}$, and κ-$(BETS)_2FeBr_xCl_{4-x}$. Among them, κ-$(BETS)_2FeBr_4$ and κ-$(BETS)_2FeCl_4$ are the first and second antiferromagnetic organic superconductors. In addition, λ-$(BETS)_2FeCl_4$ and κ-$(BETS)_2FeBr_4$ exhibit novel field-induced superconducting transitions at high magnetic fields.

The crystal structure of λ-$BETS_2MCl_4$ (M = Fe, Ga) is shown in Figure 3. BETS molecules are stacked to form a tetradic column along the a axis. There are two independent BETS molecules (A and B). There exist S (Se)···Cl distances much shorter than the van der Waals distance. Therefore, the strong π−d interaction through Cl 3p orbitals can be expected in λ-$BETS_2FeCl_4$. Since the lattice constants of $FeCl_4$ and $GaCl_4$ salts are approximately equal to each other (see Table 1), Fe and Ga atoms can be easily exchanged in an arbitrary mixing ratio. Furthermore, Cl can be exchanged to the larger Br atom to some extent. Needless to say, the Cl → Br exchange will expand the unit cell. Then, π conduction electrons in λ-$(BETS)_2MBr_xCl_{4-x}$ will feel effectively negative (chemical) pressure with increasing x. As shown in Figure 4, the unit cell parameters increase almost linearly with x. The Br distribution is not completely random, but there are preferred positions (X_2 and X_4 (see Figure 3)).[37] The occupancy probability of the Br atom is smallest in X_3 due to close contacts with neighboring BETS molecules: for example, in the case of λ-$(BETS)_2GaBr_xCl_{4-x}$ ($x = 0.54$), the occupancy probabilities of four halide positions determined by X-ray refinements were 0.24 (X_2), 0.16 (X_4), 0.09 (X_1), and 0.04 (X_3). Above $x > 2.0$, a λ-type modification cannot be obtained. Then, the $GaBr_4^-$ salt takes a modified λ-type structure with similar tetradic BETS stacks (λ'-type structure). The crystal of λ'-$(BETS)_2GaBr_4$ also belongs to the triclinic system (Table 1). The unit cell volume is about 65 Å^3 larger than that of λ-$(BETS)_2GaCl_4$, which is of course approximately

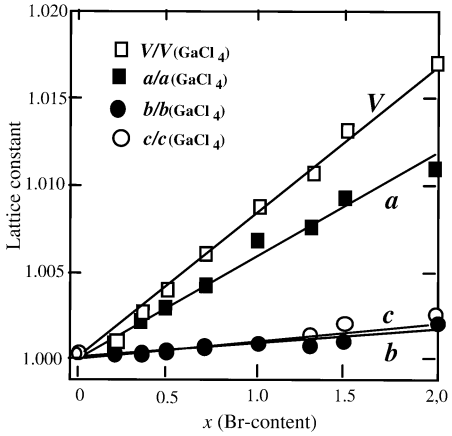

Figure 4. Bromine content (x) dependencies of the lattice constants of crystal of λ-$(BETS)_2GaBr_xCl_{4-x}$. All data are normalized by the $x = 0.0$ (λ-$(BETS)_2GaCl_4$) value.

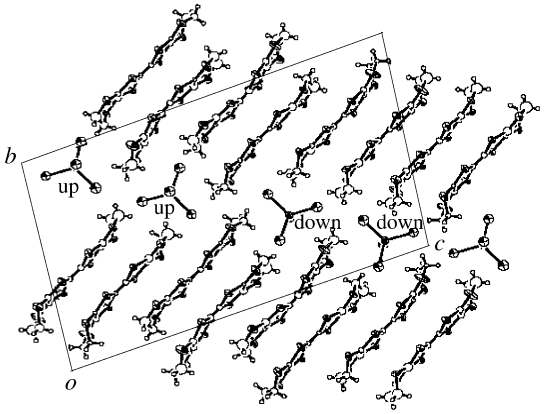

Figure 5. Crystal structure of λ''-$(BETS)_2TlBr_4$. Along the stacking direction of 8-fold BETS columns, tetrahedral $TlBr_4^-$ anions take the orientation of (up−up−down−down).

equal to a half of the difference of unit cell volumes between κ-$(BETS)_2GaCl_4$ and κ-$(BETS)_2GaBr_4$.[32] Similar to λ-$(BETS)_2GaCl_4$, the intermolecular interaction along the BETS stack indicates the strong dimeric nature of the electronic band structure. Despite the calculated Fermi surfaces and fairly high room-temperature conductivity (25 S cm^{-1}), λ'-$BETS_2GaBr_4$ exhibited a weakly semiconducting behavior and underwent an insulating transition around 50 K. The sharp susceptibility decrease below 50 K indicated the nonmagnetic insulating ground state. At high pressure (>3 kbar), the metallic behavior was observed. Recently, we have found another modified λ-type structure (λ''-type structure). As shown in Table 1, $(BETS)_2TlBr_4$ salt has a λ''-type structure.[55] Similar to the λ-type salt, λ''-$(BETS)_2TlBr_4$ has a triclinic unit cell. The unit cell volume of λ''-$(BETS)_2TlBr_4$ is about 60 Å^3 larger than twice that of λ'-$(BETS)_2GaBr_4$. As shown in Figure 5, the BETS molecules are stacked to form an 8-fold column, and tetrahedral $TlBr_4^-$ anions are arranged to take the orientation of (up−up−down−down) along the stacking direction of the 8-fold BETS column. The crystal has a fairly high conductivity but slightly semiconducting with very small activation energy (≈0.01 eV).

Since BETS tends to form a 2-D molecular arrangement, there are many salts with κ-type struc-

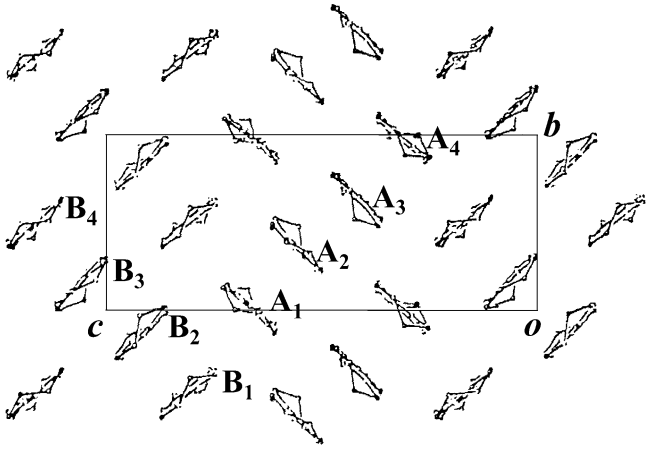

Figure 6. Molecular arrangement in $\kappa(4 \times 4)$−$(BETS)_2ClO_4(C_2H_3Cl_3)_x$. In the 2-D conduction layer, two kinds of BETS tetramers with stacking directions orthogonal to each other are arranged. Along the *a* axis, the BETS layers and anion layers containing solvent molecules (1,1,2-trichloroethane) appear alternately.

tures. Unlike the λ-type salts with a 4-fold quasi-stacking structure of donor molecules, the donor molecules in κ-type structures are no longer stacked but form face-to-face dimers rotated by about 90° with respect to each other. Besides the usual κ-type structure composed of two kinds of BETS dimers, there exist BETS salts with a unique 2-D molecular arrangement. The ClO_4^- and BF_4^- salts take $\kappa(4 \times 4)$ structures, where two kinds of BETS tetramers with stacking directions orthogonal to each other are arranged to form a 2-D conduction plane (Figure 6). The BETS layers with a $\kappa(4 \times 4)$ arrangement and anion layers containing solvent molecules (1,1,2-trichloroethane) appear alternately along the *a* axis. The tight-binding band calculation gave 2-D Fermi surfaces, which is consistent with the stable metallic state down to low temperature.[38]

Except $M(dmit)_2$ (M = Ni, Pd) complexes such as $[TTF][Ni(dmit)_2]_2$, $[(CH_3)_4N][M(dmit)_2]_2$, and $[(CH_3)_2(C_2H_5)_2N][Pd(dmit)_2]_2$,[8] almost all the molecular superconductors ever discovered are Bechgaard-type salts composed of TTF-like π donors and inorganic anions. Several years ago, Kondo et al. discovered the first example of the all-organic superconductors consisting of twinned π donor columns and π acceptor columns, $(BETS)_2(Cl_2TCNQ)$ (Figure 7a).[56,60] The CN stretching mode in vibronic spectra suggests the formal charge of Cl_2TCNQ to be −1, and the Cl_2TCNQ stack is in a quasi-1-D Mott−Hubbard insulating state. However, $(BETS)_2(Cl_2TCNQ)$ undergoes a superconducting transition around 1 K. Above 6 kbar, it takes a spin-density wave insulating state, which begins to appear below 20 K (Figure 7b).

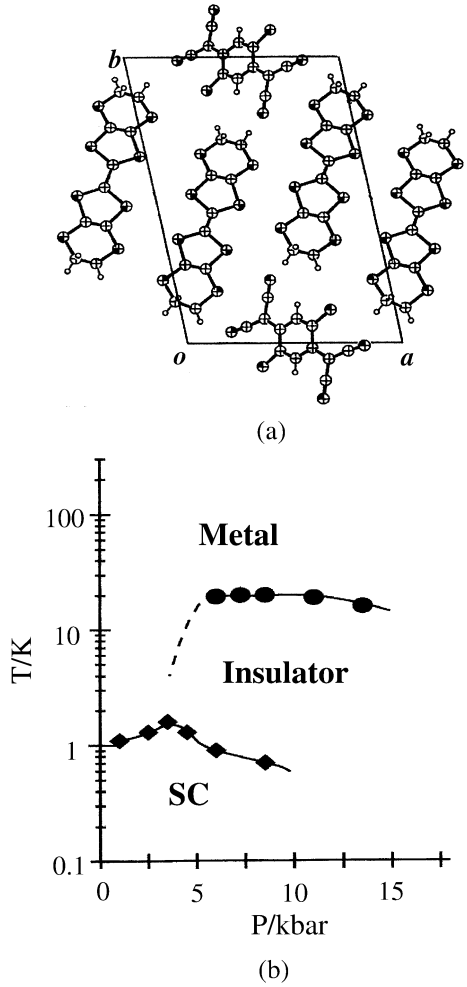

Figure 7. (a) Crystal structure of $(BETS)_2(Cl_2TCNQ)$ viewed along the *c* axis. (b) Pressure−temperature phase diagram of $(BETS)_2(Cl_2TCNQ)$. Although the organic superconductor with the segregated donor and acceptor columns have been found in $Ni(tmdt)_2$ complexes such as $[TTF][Ni(tmdt)_2]_2$ and $[EDT\text{-}TTF][Ni(dmit)_2]$,[8] $(BETS)_2(Cl_2TCNQ)$ is the first organic superconductor with segregated donor and acceptor columns of organic molecules.

3. Organic Superconductors Based on BETS

3.1. Electromagnetic Properties of λ-$(BETS)_2GaBr_xCl_{4-x}$

The crystal structure of λ-$(BETS)_2MCl_4$ (M = Ga, Fe) is shown in Figure 3, and the molecular arrangement in the *ac* conduction plane is shown in Figure 8. The large intermolecular overlap integral of the HOMO between A and B molecules (Figure 3) indicate the dimeric nature of the system (Figure 9). Therefore, similar to κ-type BEDT-TTF superconductors, the extended Hückel tight-binding band calculation based on HOMO gave the upper two and lower two bands. The essential feature of calculated 2-D Fermi surfaces was confirmed by low-temperature magnetoresistance experiments (Figure 10).[58,65] The Ga and Fe atoms can be replaced to each other, and Cl atoms can be partially exchanged to Br atoms. As mentioned before, Br exchange will expand the unit lattice and produce effectively negative chemical pressure (Figure 4). Furthermore, contrary to $GaCl_4$ salt exhibiting a superconducting transition around 5−6 K, $FeCl_4$ salt undergoes a metal−insulator (MI) transition at about 8.5 K. Thus, by the slight chemical modification of the anion site, the electrical properties of λ-$(BETS)_2Fe_xGa_{1-x}Br_yCl_{4-y}$ can be controlled over the extremely wide range (from superconducting state to insulating state). For example, as shown in Figure 11, the temperature dependencies of electrical resistivities of λ-$(BETS)_2GaBr_xCl_{4-x}$ ($x <$

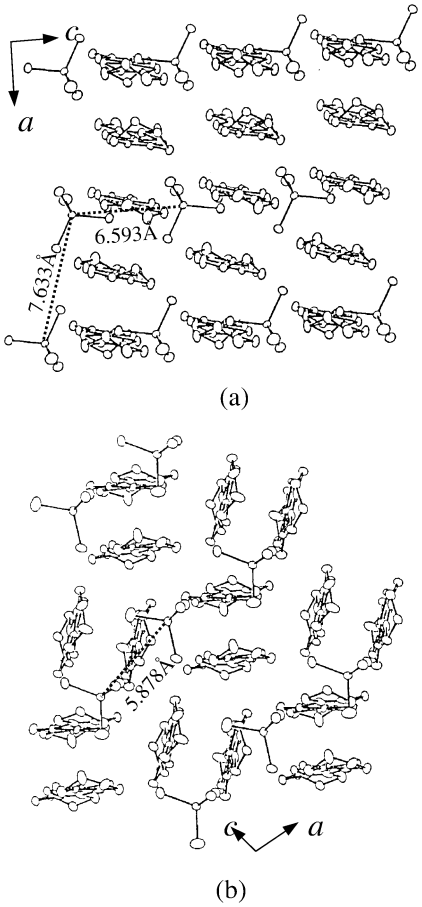

Figure 8. Arrangement of BETS molecules and tetrahalide anions viewed along the long axis of BETS molecule: (a) λ-$(BETS)_2FeCl_4$, (b) κ-$(BETS)_2FeBr_4$. The short Fe···Fe distances are given in the figure. In λ-$(BETS)_2FeCl_4$, donor molecules and anions are arranged uniformly along c. But along a, donors are arranged to form a tetradic unit, and anions with two orientations are arranged alternately. In κ-type structure, the anions are on the mirror plane perpendicular to b and arranged regularly along c.

2.0) can be changed systematically with a varying x-value. With increasing x, the characteristic round resistivity maximum around 50 K becomes prominent, and the superconducting transition temperature (T_c) slightly increases. But the Br-rich system with $x > 0.8$ becomes insulating for all the temperature region. On the other hand, in λ-$(BETS)_2GaCl_3F$ with a smaller anion, the round resistivity peak disappears, and T_c decreases. The insulating state of the Br-rich system ($x > 0.8$) is suppressed by applying pressure, and the superconducting transition appears. λ-$(BETS)_2GaBr_{1.5}Cl_{2.5}$ shows a maximum T_c of about 10 K around 3 kbar, which decreases at a higher pressure (Figure 12).[57,62] The maximum T_c tends to increase with increasing Br content. But the maximum T_c of λ-type BETS conductor will not exceed 11−12 K because the quality of Br-rich crystal of λ-$(BETS)_2GaBr_xCl_{4-x}$ becomes very poor, and the crystals with $x > 2.0$ are unobtainable. As shown in Figure 9, the intermolecular interaction C and t decreases with increasing x. Since t is very small, the decreases of the interdimer interaction C will be most important for the enhancement of the semiconducting nature of the Br-rich system. At higher x, the interaction C becomes about half of B. Then, the

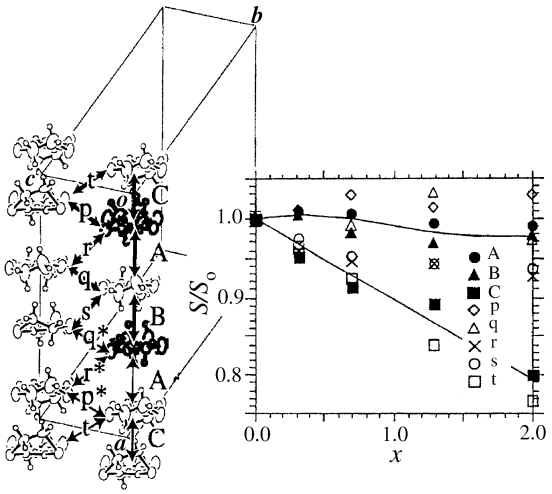

Figure 9. Molecular arrangement in λ-$(BETS)_2GaBr_xCl_{4-x}$ viewed along the long molecular axis and the x-dependence of intermolecular overlap integrals (S). The overlap integrals (A, B, C, ···, t) are normalized by the value of the $x = 0.0$ system (S_o). The intermolecular overlap integrals ($\times 10^3$) of HOMO of λ-$(BETS)_2GaCl_4$ ($x = 0.0$) are 23.8 (A), 9.84 (B), 5.76 (C), −1.27 (p), −3.07 (q), 3.69 (r), 4.83 (s), and 0.41 (t).

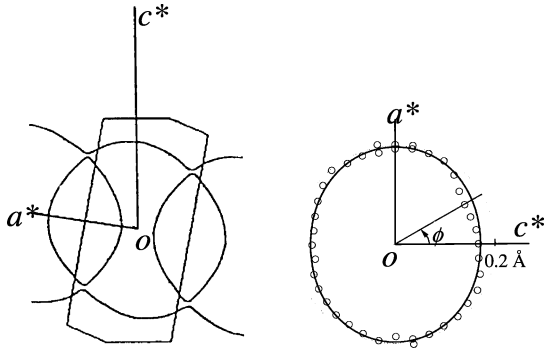

Figure 10. Calculated Fermi surface of λ-$(BETS)_2GaCl_4$ (left) and Fermi surface of κ-$(BETS)_2FeBr_4$ determined from the angular-dependent magnetoresistance oscillation (right).

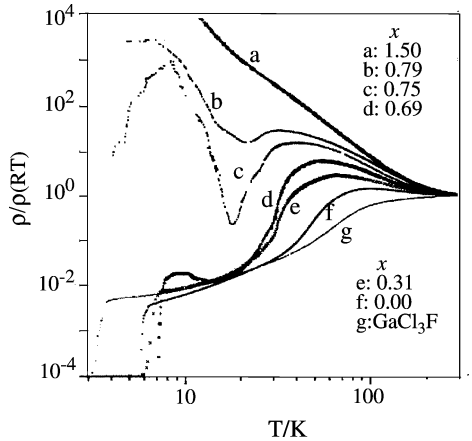

Figure 11. Temperature dependencies of electrical resistivities of λ-$(BETS)_2GaBr_xCl_{4-x}$ ($x < 2.0$) and λ-$(BETS)_2GaCl_3F$ with a smaller size anion.

system will tend to have dimer pair connected by the interdimer interaction B, which is a suitable structure to take a nonmagnetic ground state. The susceptibility of λ-$(BETS)_2GaBr_xCl_{4-x}$ is shown in Figure 13. The room-temperature susceptibility shows a slight dependence on x (4.5×10^{-4} emu/mol for $x =$

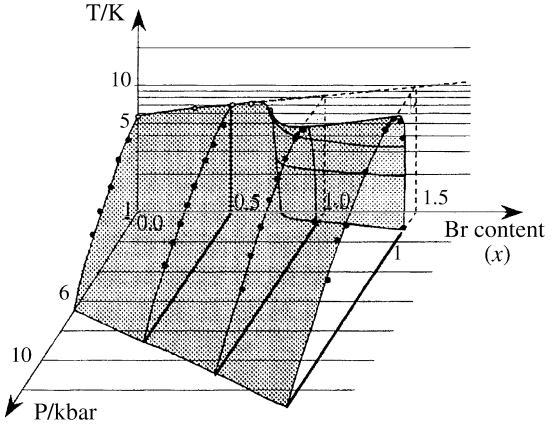

Figure 12. $T-P-x$ phase diagram of λ-$(BETS)_2GaBr_xCl_{4-x}$. The region surrounded by the shaded plane corresponds to the superconducting region. The superconductibg state of λ-$(BETS)_2GaCl_4$ survives up to 6 kbar. When $x > 0.8$, the system does not take the superconducting ground state at ambient pressure. The maximum T_c of the pressure-induced superconducting phase tends to be increased with increasing x. But T_c of λ-type BETS conductor cannot exceed 11−12 K because the λ-phase hardly exists for $x > 2.0$.

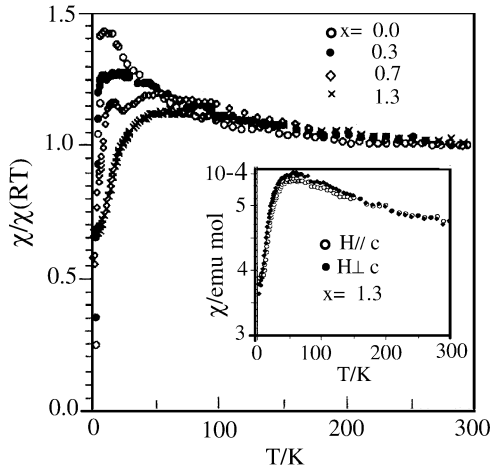

Figure 13. Magnetic susceptibility of λ-$(BETS)_2GaBr_xCl_{4-x}$ ($x = 0.0$, 0.3, 0.7, and 1.3 (polycrystalline samples)). The susceptibility is normalized at room temperature (4.5−4.9 $\times 10^{-4}$ emu/mol). The inset is the magnetic susceptibility of the oriented polycrystalline sample of λ-$(BETS)_2GaBr_{1.3}Cl_{2.7}$.

0.0 and 4.9 $\times 10^{-4}$ for $x = 1.3$). The susceptibility increases gradually with lowering temperature above 50 K, irrespective of the x-value. Of course, the superconducting system shows a strong diamagnetism, but the susceptibility begins to decrease from the temperature much higher than T_c in the Br-containing system. The remarkable susceptibility decrease is also observed in the semiconducting Br-rich system ($x > 0.8$), where the isotropic susceptibility decrease is observed below about 40 K. These features indicate some change in the magnetic state around 20−30 K. As seen from Figure 11, in the Br-rich system, the low-temperature resistivity tends to increase with decreasing temperature below about 20 K, which seems to coincide with the existence of the boundary of magnetic state. In the low-temperature insulating state of the Br-rich system, the π electrons will tend to be localized because of the strong correlation effect due to the effectively narrow

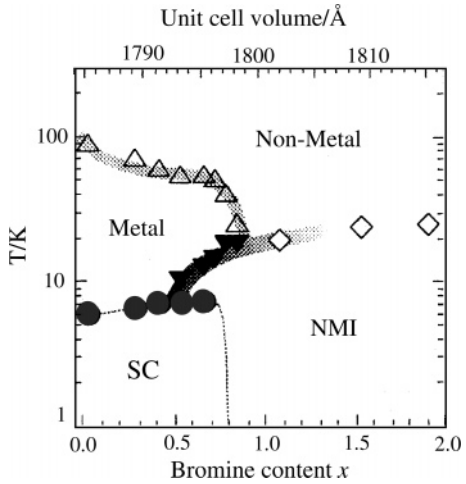

Figure 14. $T-x$ phase diagram of λ-$(BETS)_2GaBr_xCl_{4-x}$ proposed by the results of resistivity and susceptibility. The upper abscissa represents unit cell volume (bromine content x). NMI, nonmagnetic insulating state. The open diamond is the temperature where the strong susceptibility decrease is observed.

half-filled band of the system. But, it seems that the localized π spins do not appear in BETS layers at low temperature, which is consistent with the decrease of C (Figure 9) at higher x because large modulation of intermolecular interactions along the tetradic stack (A, B, A, C, ...) corresponds to the enhancement of the spin-Peiels-like character of the system. The $T-x$ phase diagram of λ-$(BETS)_2GaBr_xCl_{4-x}$ is shown in Figure 14, which corresponds to the cross-section of the $T-P-x$ phase diagram at $P = 1$ bar (Figure 12). As mentioned previously, it seems that the dimer pair tends to take singlet ground state in the Br-rich system. The Hartree−Fock analyses by Seo and Fukuyama suggest that if the on-site Coulomb interaction exceeds some critical value, antiferromagnretic spin ordering emerges and eventually leads to an insulating state that can be considered as a 2-D localized spin system.[63] λ-$(BETS)_2GaBr_xCl_{4-x}$ is considered to be located near the boundary between the antiferromagnetic phase and the spin gap phase.

3.2. κ-Type BETS Superconductors with Tetrahalide Anions

Figure 15 shows the crystal structure of κ-$(BETS)_2MX_4$ (M = Ga, Fe; X = Cl, Br). The arrangement of BETS molecules in the *ac* conduction plane is shown in Figure 8. The band structure calculation gave 2-D Fermi surfaces, which is consistent with the low-temperature magnetoresistance experiments.[58,64,65] Similar to other κ-type organic conductors, κ-type BETS conductors afford superconducting systems such as κ-$(BETS)_2FeBr_4$,[66,67] κ-$(BETS)_2FeCl_4$,[68] κ-$(BETS)_2GaBr_4$,[69] and κ-$(BETS)_2TlCl_4$.[40] These salts belong to the orthorhombic system with space group *Pnma* (see Table 1). Along the *b* axis, the BETS layers and anion layers are arranged alternately. κ-$(BETS)_2FeBr_4$ and κ-$(BETS)_2FeCl_4$ are the first and second antiferromagnetic organic superconductors, respectively. κ-$(BETS)_2GaBr_4$ undergoes a broad superconducting transition around 1 K (Figure 16), but the superconducting behavior of κ-$(BETS)_2GaCl_4$ has

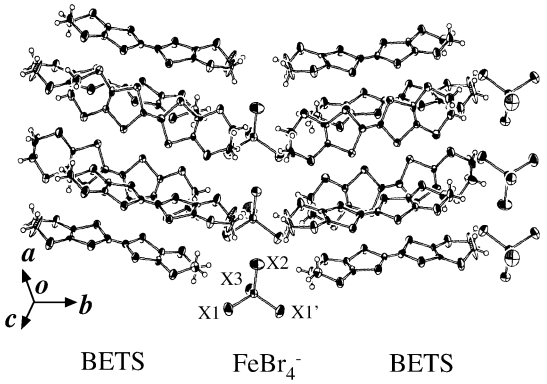

Figure 15. Crystal structure of κ-$(BETS)_2FeBr_4$. One BETS molecule and a half of $FeBr_4^-$ anion are crystallographically independent. The shortest intermolecular Se···Se, Se···S, and S···S distances are 3.796, 3.593, and 3.362 Å, respectively. The shortest Br···S and Br···Br distances are 3.693 and 4.137 Å, respectively.

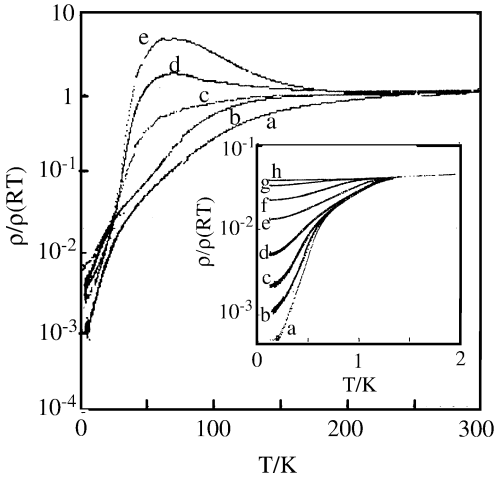

Figure 16. Resistivities of κ-$(BETS)_2GaBr_xCl_{4-x}$ [x = 0.0 (a), 1.0 (b), 2.0 (c), 3.0 (d), and 4.0 (e)]. The inset is the magnetic field dependencies of the low-temperature resistivities of κ-$(BETS)_2GaBr_4$ [H = 0 (a), 0.02 (b), 0.05 (c), 0.1 (d), 0.3 (e), 0.7 (f), 1.5 (g) and 3.0 kOe (h)].

not been observed. Similar to the λ-type Br-rich system, κ-$(BETS)_2GaBr_4$ exhibits a characteristic round resistivity maximum around 60 K, which tends to be suppressed with increasing Cl content. In the crystal of κ-$(BETS)_2GaBr_xCl_{4-x}$, the Br atoms tend to occupy the positions on the mirror plane (X2, X3 (see Figure 15)), which are relatively far from BETS layers. The accurate resistivity measurements of κ-type BETS salts with larger anions such as $FeBr_4^-$ and $GaBr_4^-$ are not so easy because the crystals frequently show small resistivity jumps. Especially, due to the destruction of the crystal around 220 K, the low-temperature resistivity measurement of $TlCl_4$ crystal was very difficult. But by coating the crystal with epoxy resin, the resistivity jump around 220 K could be fairly suppressed, and the superconducting transition was observed around 2.5 K.

These results suggest that κ-$(BETS)_2MX_4$ tends to take the superconducting ground state if the room-temperature structure can be retained down to very low temperatures. However, unlike the famous organic superconductor, κ-$ET_2[Cu(N(CN)_2)]Br$ with superconducting transition temperature of 11.6 K,[6,70] κ-$BETS_2[Cu(N(CN)_2)]Br$ does not exhibit a superconducting transition at least down to 4 K.[41] Probably, the large stability of metallic state of κ-type BETS conductors will strongly reduce the T_c of this complex. In this connection, it may be worthwhile to note that despite of the relatively weak metallic properties of BEDSe-TTF conductors, the κ-$(BEDSe\text{-}TTF)_2[Cu(N(CN)_2)]Br$ exhibits a superconducting transition at 7.5 K and 1.5 kbar, where BEDSe-TTF (= bis(ethylendiseleno)tetrathiafulvalene) is an isomer of BETS with four Se atoms in the outer six-membered ring.[71]

4. Magnetic Organic Superconductors

4.1. Electromagnetic Properties and Field-Induced Superconductivity of λ-$(BETS)_2FeCl_4$ and λ-$(BETS)_2FeBr_xCl_{4-x}$

As mentioned before, unlike a superconducting $GaCl_4$ salt, isostructural λ-$(BETS)_2FeCl_4$ undergoes a MI transition at 8.3 K (T_{MI}). Nevertheless, except for the low-temperature region, the resistivity behaviors of both salts are almost identical to each other. The resistivity slightly increases with decreasing temperature and takes a very broad maximum around 90 K, which indicates the strong correlation of π conduction electrons. Matsui and Toyota have observed the dielectric anomaly of λ-$(BETS)_2FeCl_4$ below 70 K and nonlinear electrical transport below T_{MI}.[72,73] The magnetic susceptibility measurements for the field applied parallel and perpendicular to the needle axes ($\parallel c$) of oriented thin-needle crystals revealed that the antiferromagnetic (AF) and MI transitions take place cooperatively at T_{MI}.[74] The spin−flop transition appears around 1.2 T. At first, we considered that the AF easy axis is approximately parallel to the crystallographic c axis. However, the magnetic torque experiments by Sasaki et al. showed that the AF easy axis is tilted from the c axis ($\parallel$ needle axis of the crystal) by about 30−40°.[75,76] The magnetic susceptibilities for the field parallel and perpendicular to the AF easy axis are shown in Figure 17. Below T_{MI}, the susceptibilities become anisotropic. In addition, the susceptibility shows a drop around T_{MI} for the field parallel to the easy axis. The magnitude of the susceptibility drop is 7−8% of the total susceptibility. But such a distinct anomaly was not detected for the field perpendicular to the easy axis. Since the 8% is approximately equal to the ratio of the paramagnetic susceptibility of localized S = 5/2 spin and that of S = 1/2 spin [(1 × 3)/(5 × 7) = 0.086], this susceptibility drop strongly suggests the possibility that below T_N, π conduction electrons are localized on BETS dimers and coupled antiferromagnetically with 3d (Fe^{3+}) spins.[77] Let us imagine the coupled π (S = 1/2) and d (S = 5/2) AF spin systems. Since d spins dominate the magnetic susceptibility (χ), χ can be roughly estimated from the AF coupling of d spins (AM_iM_j), where $\chi \approx 1/A$ at $T = T_N$. Then roughly speaking, for the field parallel to the easy axis, the π spin will feel the effective field of $H - (a/A)H$ through AF π−d coupling. If $a \approx 2A$, the effective field on π spin is $-H$. Then, the susceptibility will drop by about 8%. On the other hand, for the field perpendicular to the easy axis, the effective field on

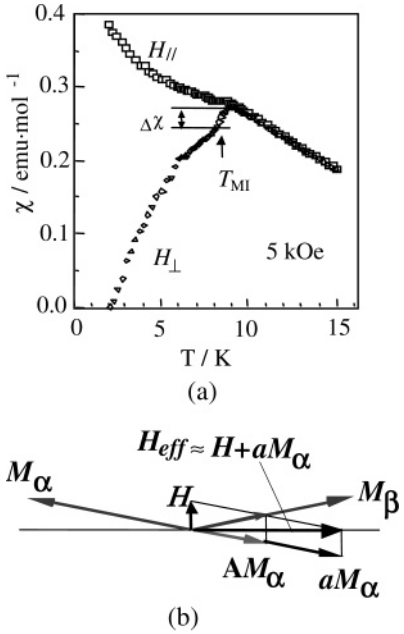

Figure 17. (a) Temperature dependencies of the susceptibilities of λ-$(BETS)_2FeCl_4$ for the fields parallel ($H_{||}$) and perpendicular ($H_\perp$) to the direction of easy axis of antiferromagnetic phase. The susceptibility for the field applied parallel to the easy axis shows a sharp drop at T_{MI} ($\Delta\chi/\chi \approx 0.07-0.08$). (b) The effective magnetic field of π spin system with applying field normal to the c axis. A and a are the antiferromagnetic coupling constant between the up and down sublattices of Fe^{3+} moments ($AM_\alpha M_\beta$) and that between π and d spin systems, respectively. When the external field (H) is perpendicular to the easy axis, the effective field on the π site will becomes approximately normal to H, when $a \approx 2A$. Then, the contributions to the magnetization from α and β spins are canceled out with each other, and the susceptibility of AF insulating phase just below T_N is approximately equal to the susceptibility of d spin system at T_N. That is, there will be no susceptibility drop for the field perpendicular to the easy axis.

π spin will be perpendicular to the external field; therefore, the contribution from π system becomes negligible (see Figure 17b). Thus, the susceptibility anomaly at T_N may be regarded as an evidence for the appearance of localized π spins on BETS dimers below T_N, where the d and π spin systems coupled antiferromagnetically. When the external field H becomes large, the magnetic moments of Fe^{3+} are forced to take ferromagnetic orientation. Then AF insulating state becomes unstable, and the localized π electrons captured by d spin systems becomes free. Consequently, the field-induced metallic state appears above 11 T.[78] λ-$(BETS)_2FeCl_4$ can be regarded as the first example of molecular conductor exhibiting a kind of colossal magnetoresistance (CMR), which is famous in the transition metal oxide conductors.[79] By applying pressure, the AF insulating state of λ-$(BETS)_2FeCl_4$ can be also suppressed, and a superconducting transition appears above 2.5 kbar ($T_c \approx 2$ K).[80]

Furthermore, Uji et al. have found the field-induced superconducting state (FISC) above 17 T for the field applied exactly parallel to the conduction plane.[81] The high-field experiments revealed the FISC to be most stabilized around 33 T (Figures 18 and 19).[82] The FISC was first observed in a pseudo-

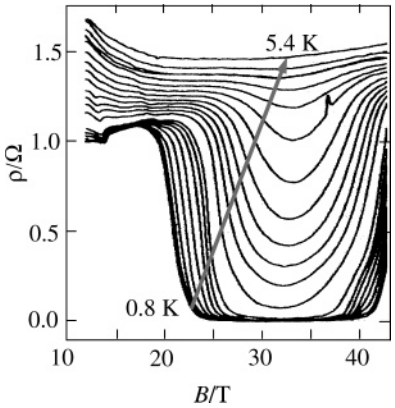

Figure 18. Resistance of λ-$(BETS)_2FeCl_4$ as a function of magnetic field applied along the in-plane c axis (±0.3°) for temperature intervals of approximately 0.25 K, between 5.4 and 0.8 K. The superconducting state develops progressively with decreasing temperature but is suppressed for field sufficiently away from (above or below) 33 T.

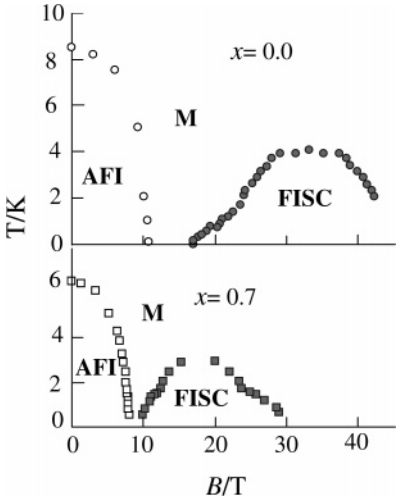

Figure 19. Temperature−magnetic field phase diagram showing the antiferromagnetic insulating (AFI), metallic (M), and field-induced superconducting (FISC) states of λ-$(BETS)_2Fe_xGa_{1-x}Cl_4$ ($x = 1.0, 0.7$). The optimal magnetic field of FISC state decreases with increasing Ga content (see also Figure 42).

ternary complex, $Eu_{0.75}Sn_{0.25}Mo_6S_{7.2}Se$, whose origin was explained on the basis of the Jaccarino−Peter compensation effect.[83,84] Similar compensation of the magnetic field in the π conduction layers will be possible in λ-$(BETS)_2FeCl_4$ because π electrons are antiferromagnetically coupled with Fe^{3+} moments with forced ferromagnetic orientation at high magnetic field (>11 T) (Figure 20).[85] The FISC means the effective field produced by π−d coupling to be 33 T, which was confirmed by the analyses of the SdH experiments.[86,87] Cépas et al. have pointed out that in the presence of the exchange field (π−d coupling), the SdH oscillation splits into two oscillation frequencies. On the basis of the experimental results obtained by Uji et al., they derived the exchange field to be about 32 T, which is in remarkable agreement with the optimal field (H_{FISC}) for superconductivity. The FISC gave a direct evidence for the existence of a considerable interaction between π metal electrons in organic donor layers and localized magnetic moments in the anion layers, which has not been

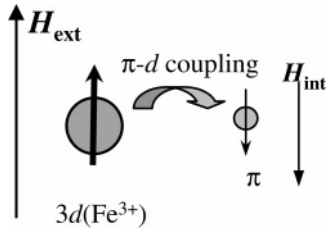

Figure 20. Schematic picture of the Jaccarino−Peter (JP) effect. The large magnetic moment of Fe^{3+} ($S = 5/2$) ions is forced to orient parallel to the strong external field (H_{ext}). Owing to the antiferromagnetic $\pi-d$ coupling, the internal field of H_{int} antiparallel to H_{ext} is produced on the π conduction layer.

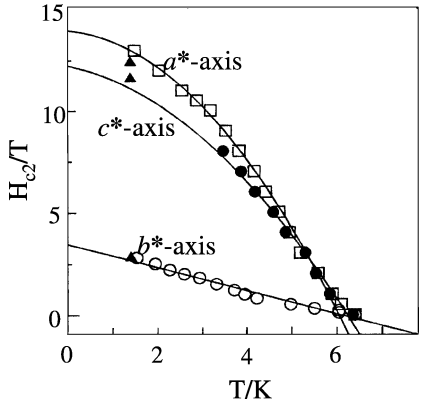

Figure 21. $H_{c2}-T$ phase diagram of λ-$(BETS)_2GaCl_4$. H_{c2} was determined at the midpoint of the resistance drop at the superconducting transition.

observed clearly in other organic/inorganic composite magnetic conductors. Since H_{c2} of the isostructural nonmagnetic organic superconductor λ-$(BETS)_2GaCl_4$ is about 12 T for the field parallel to the c axis (Figure 21),[88] it seems natural that FISC starts to appear around 20 T ($\approx H_{FISC} - H_{c2}(GaCl_4)$). In addition, it should be also noted that the possibility of more exotic superconducting state (inhomogeneous FFLO state) has been suggested in λ-$(BETS)_2FeCl_4$.[82,89−91]

The broad resistivity maximum around 90 K in λ-$(BETS)_2FeCl_4$ becomes prominent in λ-$(BETS)_2FeBr_xCl_{4-x}$ with increasing x (Figure 22). The resistivity behavior of λ-$(BETS)_2FeBr_xCl_{4-x}$ quite resembles that of nonmagnetic λ-$(BETS)_2GaBr_xCl_{4-x}$ salt except the low-temperature region, which suggests that the π electron state is essentially the same to that of the λ-$(BETS)_2GaBr_xCl_{4-x}$ salt. The increase of T_{MI} and the enhancement of the resistivity maximum at higher x indicate that π electrons tend to be localized with increasing x. T_{MI} of λ-$(BETS)_2FeBr_{0.7}Cl_{3.3}$ is about 18 K, which is more than twice the T_{MI} of λ-$(BETS)_2FeCl_4$ (8.3 K).[92] At $x > 0.8$, λ-$(BETS)_2FeBr_xCl_{4-x}$ becomes a semiconductor down to a low temperature. However, as expected, the chemical pressure dependence of the resistivity can be almost reproduced by applying real pressure. Above 4 kbar, the system becomes metallic down to 4 K. The magnetic susceptibility measured on the oriented thin needle crystals (needle axis $\|c$) revealed that the easy axis rotates with increasing Br content (Figure 23). Unlike λ-$(BETS)_2FeCl_4$ exhibiting susceptibility drop and spin−flop behavior for the field parallel to c, λ-$(BETS)_2FeBr_{0.65}Cl_{3.35}$ shows spin−flop behavior for

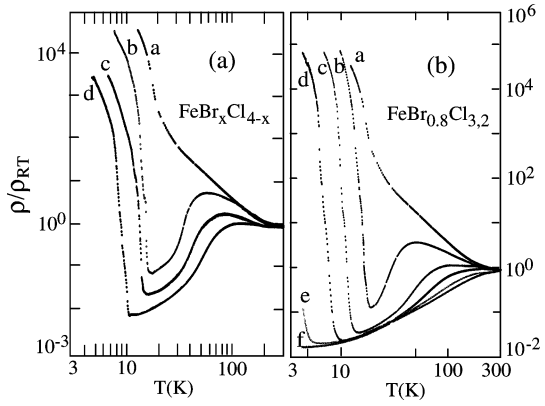

Figure 22. (a) (Left) temperature dependence of the resistivity of λ-$(BETS)_2FeBr_xCl_{4-x}$ [$x = 0.8$ (a), 0.65 (b), 0.6 (c), and 0.0 (d)] down to 4.2 K. (b) (Right) temperature dependence of the resistivity of λ-$(BETS)_2FeBr_{0.8}Cl_{3.2}$ at 1 bar (a), 1.1 kbar (b), 1.5 kbar (c), 2.0 kbar (d), 3.0 kbar (e), and 4.0 kbar (f). Considering the pressure-induced superconductivity of λ-$(BETS)_2FeCl_4$ around 3 kbar, λ-$(BETS)_2FeBr_{0.8}Cl_{3.2}$ will show the superconducting transition above 4 kbar at low temperatures (see also Figure 30).

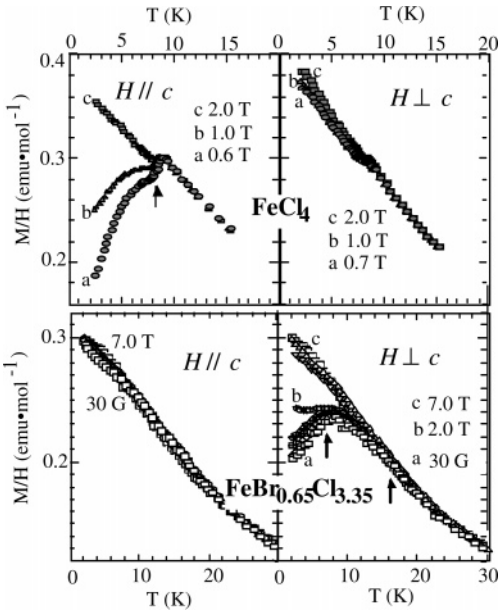

Figure 23. Temperature dependence of the susceptibility of oriented polycrystalline samples of λ-$(BETS)_2FeCl_{4-x}Br_x$ ($x = 0$ and 0.65) for the fields parallel and perpendicular to axis c. For $x = 0$, the arrow indicates the cooperative MI and antiferromagnetic transition temperature. For $x = 0.65$, two arrows indicate the antiferromagnetic and MI transition temperatures (T_N, T_{MI}).

the field perpendicular to c, which indicates that the easy axis of AF insulating phase rotates by about 90° with increasing Br content.[92] Furthermore, the temperature below which the susceptibility of λ-$(BETS)_2FeBr_{0.65}Cl_{3.35}$ shows spin−flop behavior (7.5 K) is about a half of the T_{MI} in λ-$(BETS)_2FeBr_{0.65}Cl_{3.35}$ (16 K). That is, in a Br-rich system, π and d electron systems tend to be uncoupled, and the MI transition temperature and antiferromagnetic transition tends to be separated. This means that the unique coupled MI and AF transition observed in λ-$(BETS)_2FeCl_4$ is related to the fact that the π electron instability and magnetic transition happen to occur around the same temperature.

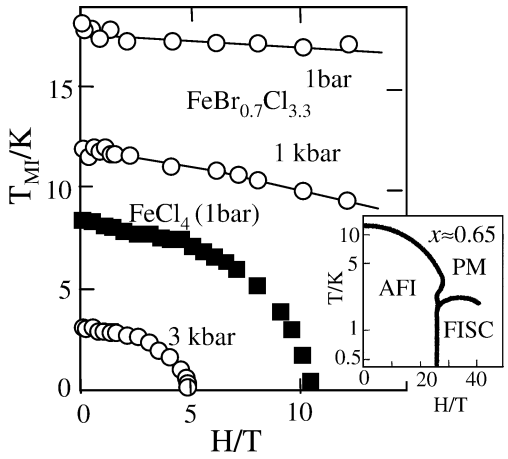

Figure 24. Magnetic field dependence of T_{MI} of λ-$(BETS)_2FeBr_{0.7}Cl_{3.3}$ (open circles) determined by resistivity measurements at 1 bar, 1 kbar, and 3 kbar. The data of λ-$(BETS)_2FeCl_4$ are presented for comparison (closed square). A rough sketch of the $T-H$ phase diagram of λ-$(BETS)_2FeBr_{0.65}Cl_{3.35}$ at ambient pressure is also presented in the small square: AFI = antiferromagnetic insulating phase, PM = paramagnetic metal phase, and FISC = field-induced superconducting phase.

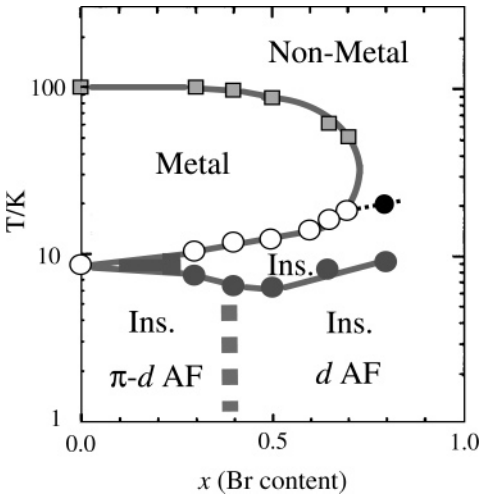

Figure 25. $T-x$ phase diagram of of λ-$(BETS)_2FeBr_xCl_{4-x}$. The squares indicate the temperature corresponding to the resistivity maximum. The open circles correspond to T_{MI}, and the black circle corresponds to the temperature of the semiconductor−insulator transition. The gray circles indicate the temperature of antiferromagnetic ordering of Fe^{3+} moments (T_N). The thick broken line around $x = 0.4$ suggests the boundary of strong and weak coupling between π and d electron systems.

Since the $\pi-d$ coupling seems to be weakened with increasing Br content and the π electron system tends to be nonmagnetic at low temperature, the MI transition temperature is considered to become independent of the external field. In fact, unlike λ-$(BETS)_2FeCl_4$ showing a strong magnetic field dependence of T_{MI} to result in the field-restored metallic state above 11 T, T_{MI} of λ-$(BETS)_2FeBr_xCl_{4-x}$ ($x \approx 0.7$) shows very weak magnetic-field dependence up to 12 T (Figure 24).[92] However, Uji et al. have recently found that T_{MI} of λ-$(BETS)_2FeBr_{0.65}Cl_{3.35}$ decreases rapidly above 20 T, and the FISC state appears around 32 T.[93] As seen from Figure 24, T_{MI} decreases with increasing magnetic field at high pressure. T_{MI} decreases with pressure and becomes about 8 K around 2 kbar, which is approximately equal to T_{MI} of λ-$(BETS)_2FeCl_4$ at ambient pressure.[92] Then, it is quite natural that the field restored metallic state is observed around 11 T.[92] At higher pressure, T_{MI} decreases further, and the field restored metallic state is observed at lower field (for example, 5 T at 3 kbar (see Figure 24)). However, the reason that T_{MI} of the Br-rich system decreases at high magnetic field is not clear. As seen from Figure 13, π electron system in Br-rich λ-$(BETS)_2GaBr_xCl_{4-x}$ system tends to approach to the nonmagnetic state at low temperature, while the strong magnetic field will favor the paramagnetic state (or metallic state). Consequently, T_{MI} will be suppressed at a high magnetic field, and the coupling of the instabilities of the π and d electron systems will be realized. It might be possible that the spin gap state of the Br-rich system predicted by Seo and Fukuyama[63] is suppressed by a strong magnetic field.

Considering the separation of MI and AF transition temperatures in a Br-rich system, $\pi-d$ coupling seems to be weakened with increasing Br content. On the other hand, the $\pi-d$ interaction through the intermolecular overlapping of the d-like orbital (3p(Cl)−d (or 4p(Br)−d) mixing orbital) of FeX_4^- and the π molecular orbital of BETS will be enhanced with increasing of Br content due to the large electron cloud of Br atom. As mentioned previously, the FISC phase of λ-$(BETS)_2FeBr_{0.65}Cl_{3.35}$ is observed around 32 T, which is approximately equal to the optimal magnetic field of FISC phase of λ-$(BETS)_2FeCl_4$.[93] That is, the effective magnetic field on BETS layers produced by ferromagnetically oriented Fe^{3+} moments seems to be almost independent of Br content. The temperature composition ($T-x$) phase diagram of λ-$(BETS)_2FeBr_xCl_{4-x}$ is shown in Figure 25. The general feature of phase diagram at $T > 10$ K quite resembles that of λ-$(BETS)_2GaBr_xCl_{4-x}$ (Figure 14), where the electrical properties are determined only by the π electron system. But below 10 K, $\pi-d$ coupling becomes important, and the AF insulating region appears around the region where the superconducting phase is observed in λ-$(BETS)_2GaBr_xCl_{4-x}$.

4.2. Superconductor-to-Insulator Transition of λ-$(BETS)_2Fe_xGa_{1-x}Cl_4$

As mentioned previously, λ-$(BETS)_2FeCl_4$ undergoes a MI transition, whereas the λ-$(BETS)_2GaCl_4$ undergoes a SC transition. It is well-known that the introduction of impurity in the 2-D organic superconductors such as β-$(BEDT\text{-}TTF)_2I_3$ strongly suppresses the superconducting transition temperature even in the case of nonmagnetic impurity (IBr_2^-) due to the Anderson localization effect.[94] Therefore, one might consider that the introduction of a small amount of magnetic $FeCl_4^-$ anions in λ-$(BETS)_2GaCl_4$ will destroy the superconductivity.[95] However, we have found many novel superconducting phenomena in λ-$(BETS)_2Fe_xGa_{1-x}Cl_4$.

Crystals of λ-$(BETS)_2Fe_xGa_{1-x}Cl_4$ were prepared electrochemically from 10% ethanol-containing chlorobenzene solutions of BETS and mixed $(Et_4N)(FeCl_4)$ and $(Et_4N)(GaCl_4)$ supporting electrolytes in the

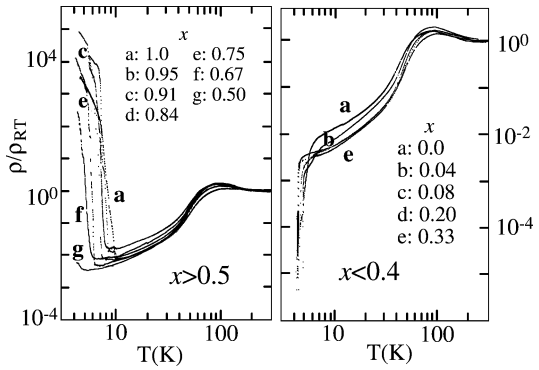

Figure 26. Temperature dependence of the resistivity of λ-$(BETS)_2Fe_xGa_{1-x}Cl_4$ at $T > 4.2$ K. In the Fe-rich system ($x > 0.5$), T_{MI} decreases systematically with increasing Ga content (a → b → c → d → e → f → g), and in the Ga rich system ($x < 0.5$), T_c decreases slightly but systematically with increasing Fe content (a → b → c → d → e). Around $x = 0.5$, T_{MI} and T_c become almost equal to each other.

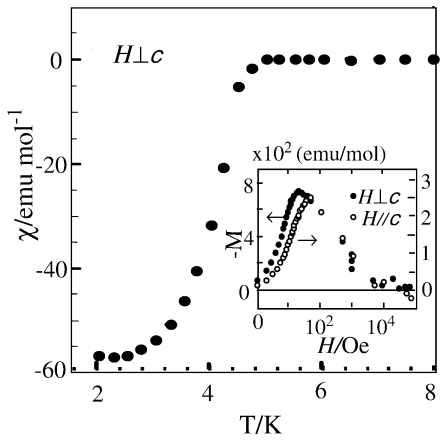

Figure 27. Temperature dependence of the susceptibilities of the oriented thin needle crystals of λ-$(BETS)_2GaCl_4$. The applied magnetic field is 2 Oe. The demagnetization field effect is not included. The inset is the field dependence of the magnetization at 2 K showing the type II behavior of the superconducting state.

appropriate proportions. The x values were determined by EPMA (electron probe microanalysis) and/or X-ray refinements of the atomic population of the anion site, which were in good agreement with the Fe/Ga ratio in the starting solution, except for $x < 0.2$ and $x > 0.8$, where the minority component (Fe^{3+} for $x < 0.2$ and Ga^{3+} for $x > 0.8$) tended to be included in the crystal.

As shown in Figure 26, the Fe-rich phases of λ-$(BETS)_2Fe_xGa_{1-x}Cl_4$ ($x > 0.5$) undergo a sharp MI transition. The transition temperature T_{MI} of λ-$(BETS)_2Fe_xGa_{1-x}Cl_4$ decreases with decreasing Fe content (x). By contrast, the Ga-rich phases ($x < 0.5$) exhibits a superconducting transition. T_c slightly decreases with increasing Fe content. If the crystal of λ-$(BETS)_2Fe_xGa_{1-x}Cl_4$ is composed of the domains of λ-$(BETS)_2FeCl_4$ and λ-$(BETS)_2GaCl_4$, the MI transition temperature observed in Fe-rich crystal will retain about 8 K independently of the x value, and the superconducting volume fraction of the Ga-rich system will decrease with x. Of course, as seen from Figure 26, T_{MI} showed continuous change. In addition, the diamagnetic susceptibilities of λ-$(BETS)_2Fe_xGa_{1-x}Cl_4$ exhibiting superconducting transitions gave almost a full Meissner value at low temperature. The susceptibility of the oriented polycrystalline sample of λ-$(BETS)_2GaCl_4$ for the field ($H = 2$ Oe) perpendicular to the needle axes of the crystals ($\parallel c$) was about −57 emu/mol at low temperature, which is 1.15 times as large as the full Meissner value of the system (≈ −50 emu/mol), where the demagnetizing field effect was not included (see Figure 27). The inset of Figure 27 indicates the typical type-II behavior. The lower critical magnetic field (H_{c1}) was about 12 and 8 Oe for the field parallel and perpendicular to the c axis. On the other hand, as mentioned before, the upper critical field (H_{c2}) is about 12 and 3 T for the field parallel and perpendicular to the c axis (Figure 21).[88] Similar to λ-$(BETS)_2GaCl_4$, λ-$(BETS)_2Fe_{0.27}Ga_{0.73}Cl_4$ showed a large diamagnetic susceptibility (−62 emu/mol) for $H\perp c$, which is apparently about 25% larger than the full Meissner value. Continuous decrease of T_{MI} with decreasing x and the almost perfect diamagnetism of λ-$(BETS)_2Fe_xGa_{1-x}Cl_4$ suggest the homogeneity of the crystal of

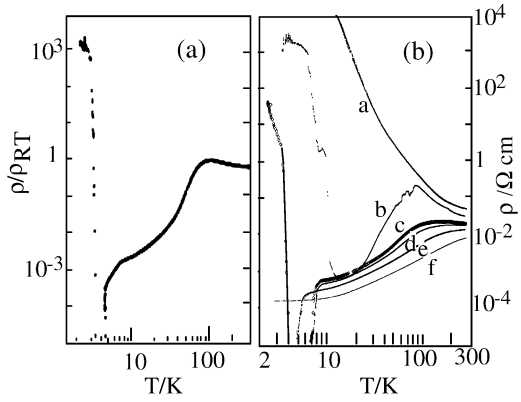

Figure 28. Two examples of the crystals of λ-$(BETS)_2Fe_xGa_{1-x}Cl_4$ showing successive metal → superconductor → insulator transitions. (a) Temperature dependence of the resistivity of λ-$(BETS)_2Fe_{0.45}Ga_{0.55}Cl_4$ at ambient pressure, which shows very narrow superconducting temperature region around 4 K. (b) The temperature dependence of the resistivity of λ-$(BETS)_2Fe_{0.5}Ga_{0.5}BrCl_3$ at 1 bar (a), 1.2 kbar (b), 2 kbar (c), 2.8 kbar (d), 3.6 kbar (e), and 7.8 kbar (f). Around 2 kbar, the system has a superconducting phase at 3.5−7 K sandwiched by low-temperature insulating and high-temperature metallic phases.

λ-$(BETS)_2Fe_xGa_{1-x}Cl_4$ ($0 < x < 1.0$). Around $x = 0.5$, T_{MI} and T_c are equal to each other. Then, it may be imagined that the insulating ground state will slip under the superconducting region at $x < 0.5$. At the borderline, where x is a slightly smaller than 0.5, the compound still undergoes a SC transition, which is followed by an unprecedented superconductor−insulator (SC−I) transition at lower temperature (i.e., below liquid helium temperature) (Figure 28). Similar to the MI transition at $x > 0.5$, the SC−I transition exhibits a hysteresis, indicating its first-order nature. Thus, λ-$(BETS)_2Fe_xGa_{1-x}Cl_4$ will undergo successively a superconducting transition and an unprecedented superconductor−insulator (SC−I) transition with lowering temperature at $0.35 < x < 0.5$.[96] In contrast to the SC transition, the SC−I transition exhibits an hysteresis. The *ac* susceptibility of the oriented polycrystalline sample of λ-$(BETS)_2Fe_xGa_{1-x}Cl_4$ ($x \approx 0.47$) showed a large diamagnetism of about −38 emu/mol around 4 K, which approximately

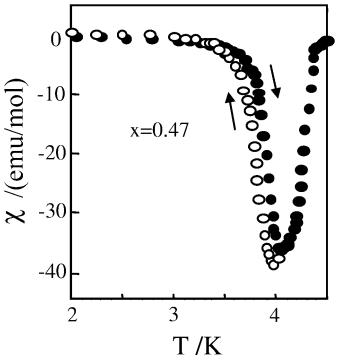

Figure 29. *ac* susceptibility of the oriented polycrystalline sample of λ-$(BETS)_2Fe_{0.47}Ga_{0.53}Cl_4$ exhibiting the successive metal → superconductor → insulator transitions around 4 K. The *ac* magnetic field of 0.1 Oe was applied perpendicular to *c*. The crystals were cooled to 4 K at zero-field.

corresponds to 75% of the perfect Meissner value (Figure 29). Considering the possible distribution of *x* values in the polycrystalline sample and the very narrow superconducting temperature region, this χ value is extremely large and shows a bulk nature of this unprecedented SC−I transition. With decreasing temperature, the large diamagnetism disappears, indicating the normal insulating ground state (Figure 29). In the field-heating process from 2 K, the large decrease of the susceptibility and the recovery of the susceptibility corresponding to the successive insulator → superconductor → metal transitions were observed. A spin−flop transition was observed around 0.6 T at 2 K for the field parallel to the *c* axis, indicating that an insulating ground state of λ-$(BETS)_2Fe_xGa_{1-x}Cl_4$ takes a π−d coupled antiferromagnetic insulating state irrespective of the *x* value ($x > 0.35$). Similar to λ-$(BETS)_2FeCl_4$ exhibiting a superconducting transition at high pressure, the Fe-rich system with AF insulating ground state at ambient pressure showed a superconducting transition at high pressure. The temperature (*T*) −pressure (*P*) composition (or Fe content (*x*)) phase diagram of λ-$(BETS)_2Fe_xGa_{1-x}Br_yCl_{4-y}$ is given in Figure 30, where the negative pressure region (*T*−*x*−*y* (Br content)) is also included. As mentioned before, the system with large Br content is an insulator. But, it becomes a superconductor by applying pressure. λ-$(BETS)_2Fe_{0.5}Ga_{0.5}BrCl_3$ with semiconducting properties at ambient pressure due to the large Br content showed a SC−I transition around 2 kbar. The temperature region of superconducting phase sandwiched by high-temperature metallic and low-temperature insulating phases was much wider as compared with that of λ-$(BETS)_2Fe_xGa_{1-x}Cl_4$ owing to the enhancement of T_c in Br-rich system (Figure 28).

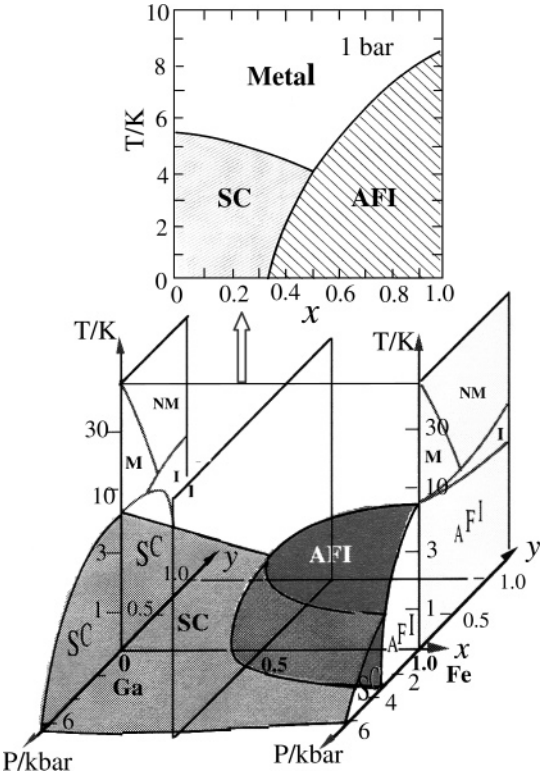

Figure 30. Temperature (*T*), composition (*x*), pressure (*P*), or Br content (*y*) corresponding to negative chemical pressure phase diagram of λ-$(BETS)_2Fe_xGa_{1-x}Br_yCl_{4-y}$: SC = superconductor, AFI = antiferromagnetic insulator, M = metal, I = insulator, and NM = nonmetallic state. The *T*−*y* phase diagram at $x = 0.0$ is the same as the phase diagram shown in Figure 14, and the *T*−*y* phase diagram at $x = 1.0$ is the same to that shown in Figure 25. The upper Figure is the *T*−*x* phase diagram of λ-$(BETS)_2Fe_xGa_{1-x}Cl_4$ at ambient pressure.

4.3. Antiferromagnetic Organic Superconductors, κ-$(BETS)_2FeBr_4$ and κ-$(BETS)_2FeCl_4$

In λ-type crystals, the space available for the accommodation of anions seems to be strictly fixed because the anion site is closely surrounded by neighboring BETS molecules. Therefore, the anions with the sizes suitable for the formation of λ-type structure seem to be very limited. Only $GaCl_4^-$ and $FeCl_4^-$ have been known to construct the λ-type structure. The larger $GaBr_nCl_{4-n}^-$ and $FeBr_nCl_{4-n}^-$ anions ($n > 2$) can be partially included in the λ-type structure. In contrast, the κ-type structure can accommodate many anions such as PF_6^-, AsF_6^-, MX_4^- (M = Ga, Fe, In, Tl; X = Cl, Br) and Cl^- (Table 1). Almost all the κ-type salts ever obtained showed metallic behavior at low temperature. And as mentioned before, some salts with tetrahalide anions ($GaBr_4^-$, $TlCl_4^-$, $FeBr_4^-$, and $FeCl_4^-$ salts) undergo superconducting transitions. However, as reported before,[32] the salts with large size anions such as $GaBr_4^-$, $InCl_4^-$, and $FeBr_4^-$ exhibit a gradual resistivity increase with lowering temperature at high-temperature region suggesting the strong correlation of π electrons, which is consistent with negative chemical pressure effect.

The plate-shaped crystals of κ-$(BETS)_2FeBr_4$ belong to the orthorhombic system with space group *Pnma* (Figures 8 and 15). The 2-D conduction layers composed of the BETS dimers and the $FeBr_4^-$ anion layers are arranged alternately along the *b* axis. In the anion layer, the shortest Fe−Fe distance is 5.878 Å along the *a* axis and 8.504 Å along the *c* axis. The shortest Br−Br distance between $FeBr_4^-$ anions is 4.137 Å along the *a* axis, which is much shorter than that along the *c* axis, 4.637 Å. However, these distances are still longer than the sum of the van der

Waals radii of bromines (3.90 Å). From these results, the direct intermolecular interaction between $FeBr_4^-$ anions is considered to be stronger along the *a* axis than along the *c* axis. There are several short Br−S contacts almost equal to the sum of the van der Waals radii of bromine and sulfur atoms (3.80 Å) between BETS and the anion molecules. The shortest Br−S distance is 3.708 Å. On the other hand, in λ-$(BETS)_2FeCl_4$, there are several short contacts between BETS and $FeCl_4^-$ anion: Cl···S contacts = 3.417, 3.642, 3.648, and 3.674 Å and Cl···Se contact = 3.528 Å, where the Cl···S and Cl···Se van der Waals distances are 3.65 and 3.80 Å, respectively. Thus, the π−d interaction of κ-$(BETS)_2FeBr_4$ will be fairly weaker than that of λ-$(BETS)_2FeCl_4$ salt. The temperature dependence of the lattice parameters of κ-$(BETS)_2FeBr_4$ indicated the existence of some structural anomaly in the temperature range 60−140 K. Around 100 K, the *b* parameter showed a hysteresis-like behavior (i.e., there was a decrease of the *b* parameters for about 0.1 Å between 110 and 90 K at cooling, and practically the same reverse change between 120 and 140 K at warming run). On the other hand, the *a* parameter of the lattice had a remarkable change at around 60 K both for cooling and for warming cycles. The results of the temperature dependence of lattice constants described previously indicate the presence of the structure transformation of κ-$(BETS)_2FeBr_4$ in the temperature range 60−140 K.[67] As mentioned before, the tight-binding band calculation gave 2-D Fermi surfaces. Low-temperature magnetoresistance experiments on κ-$(BETS)_2MX_4$ (MX_4 = $GaCl_4$, $FeCl_4$, and $FeBr_4$) gave α and β orbits, which corresponds to the cross-section areas of 20 and 100% of 1sf BZ.[98,99] The β-orbit showed 2.3% splitting.

Magnetic susceptibilities at 100−300 K could be well-fitted by the Curie−Weiss plot, where χT was almost constant: $\chi = C/(T - \theta)$; $C = 4.70$ K emu mol^{-1} and $\theta = -5.5$ K.[67] The Curie constant (C = 4.70 K emu mol^{-1}) was approximately equal to 4.38 K emu mol^{-1} [= $N_A g^2 \mu_B S(S + 1)$] expected for the $S = 5/2$ localized spin system with $g = 2.0$. Figure 31 shows the temperature dependence of susceptibilities at 2−10 K. The susceptibilities ($\chi_{\|a}$, $\chi_{\|b}$, and $\chi_{\|c}$) take a maximum around 3 K. Then, a sharp decrease was observed around 2.5 K only when the magnetic field was applied in parallel to the *a* axis, and $\chi_{\|b}$ and $\chi_{\|c}$ tended to be constant with lowering temperature. These results indicate the simple antiferromagnetic ordering of Fe^{3+} spins around 2.5 K (T_N; Néel temperature) with the easy spin axis parallel to the crystallographic *a* axis. The *ac* susceptibility was also measured from 60 mK to 7 K, where sharp decrease of χ showing the onset of the superconducting transition was observed around 1 K. A metamagnetic transition was observed around 1.6 T for $H\|a$ (easy axis of AF structure). The magnetization increased rapidly and saturated to the value of the $S = 5/2$ spin system at 30 kOe. When the magnetic field was applied in parallel to the *b* and *c* axes, the magnetization increased linearly with increasing external field and tended to be saturated around 60 kOe. The metamagnetism suggests the existence of ferromagnetic sublattices coupled antiferromagnetically to each other. Since the kinetic exchange interaction through intermolecular overlapping of frontier orbitals produces the antiferromagnetic interaction, the possibility of the ferromagnetic sublattice will be hardly imagined in this system if only one kind of magnetic moments (Fe^{3+}) are considered. The estimation of π−d interaction based on the simple extended-Hückel molecular orbital calculation was reported by Mori and Katsuhara.[100]

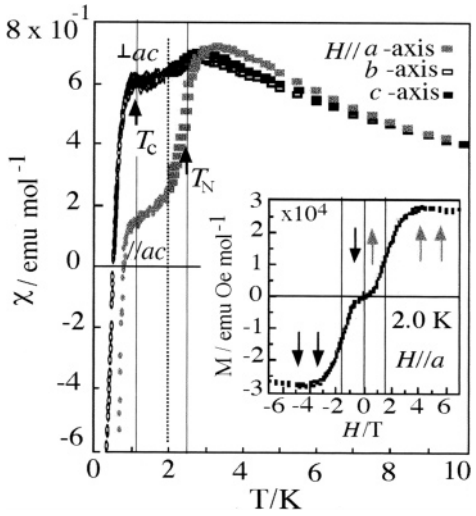

Figure 31. Magnetic susceptibility of κ-$(BETS)_2FeBr_4$. The SQUID measurements were made on the single crystal down to 2 K below which *ac* susceptibility measurements were made by using the oriented polycrystalline sample down to 60 mK for the field parallel and perpendicular to the *ac* conduction plane. Both antiferromagnetic and superconducting transitions were observed around 2.5 and 1 K. The inset is the magnetization curve for the field applied parallel to the easy axis of AF phase ($\|a$) at 2 K. The metamagetic transition was observed around 1.6 T.

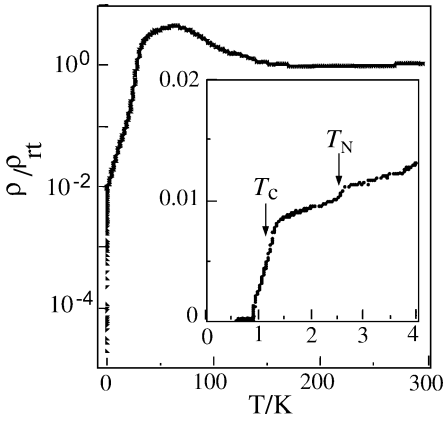

Figure 32. Temperature dependence of the resistivity of κ-$(BETS)_2FeBr_4$. The broad resistivity maximum indicating the strong correlation of the π conduction electron was observed around 60 K. The inset is the low-temperature behavior of the resistivity. The resistivity step at 2.5 K corresponds to the AF ordering of Fe^{3+} moments. The superconducting temperature was observed around 1.1 K.

Contrary to the normal metal behavior of κ-$BETS_2FeCl_4$, the resistivity of κ-$BETS_2FeBr_4$ decreased very slowly down to about 200 K and showed a broad peak around 60 K, below which resistivity decreased very rapidly (Figure 32). The resistivity decreased with lowering temperature even below 4 K. A resistivity

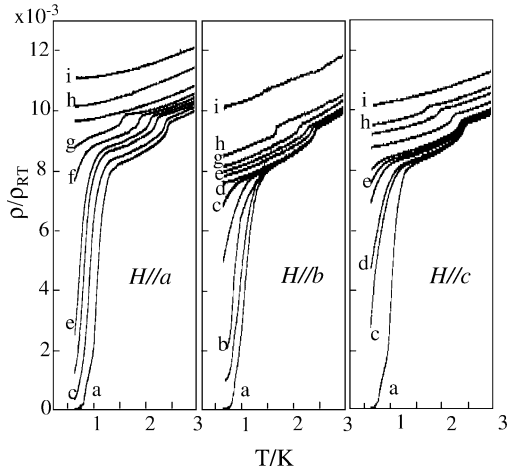

Figure 33. Temperature dependencies of the resistivities of κ-$(BETS)_2FeBr_4$ at 0.6−3.0 K measured under magnetic field applied along the $a-c$ axes at 0 (a), 0.8 (b), 2 (c), 5 (d), 10 (e), 12 (f), 15 (g), 30 (h), and 40 kOe (i) (the magnetic field is increases from the lowest line (a) to the highest line (i), but the magnetic fields are not indicated to all the resistivity lines due to the limitation of the space). Owing to the metamagnetism, the resistivity behavior under magnetic field becomes very anisotropic in the 2-D conduction plane. The resistivity changes sharply around 12 kOe for $H\|a$ but changes continuously around 5 kOe for $H\|c$. For the field perpendicular to the *ac* conduction plane, the superconducting state is broken around 0.7 kOe.

step was observed around 2.5 K where the antiferromagnetic ordering of Fe^{3+} spins is observed. This resistivity anomaly is one of the evidences for the $\pi-d$ interaction in organic conductors. Then the superconducting transition was observed around 1.1 K. By applying weak magnetic field (≈70 Oe) perpendicular to the conduction plane at 0.6 K, the superconducting state was broken. The existence of antiferromagnetic organic superconductors (AFSC) was thus disclosed for the first time. As shown in Figure 33, when applying the magnetic fields along the easy axis of the antiferromagnetic transition ($H\|a$), the resistivity drop at T_N (2.5 K) under zero magnetic field shifted quickly to the lower temperatures and disappeared at 18 kOe. On the other hand, when we applied the magnetic fields along the *b* and *c* axes, the temperature shifts of the resistivity drop were very small up to 10 kOe, and then the drop gradually moved to the lower temperatures and vanished at 40 kOe. These results well correspond to the metamagnetic behavior of this salt and clearly show the coexistence of the antiferromagnetism and superconductivity below 1.1 K.

The specific heat measurements performed down to about 0.9 K at zero magnetic field showed a large anomaly characterized by a sharp λ-type peak at about 2.4 K, which corresponds to the antiferromagnetic transition temperature (Figure 34).[67] The entropy [$S(T)$] gradually increased with increasing temperature, and S reaches to R ln 6 (= 14.9 J mol^{-1} K^{-1}), corresponding to the full entropy from the degenerate freedom of $S = 5/2$ spins, at about 3.8 K. By applying magnetic fields perpendicular to the *ac* lane, the peak position shifted to lower temperatures, which agrees well with the results, indicating the suppression of T_N by the external field (Figure 33).

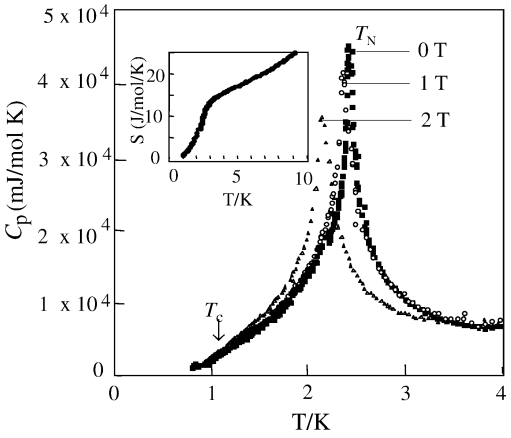

Figure 34. Temperature dependence of specific heat of κ-$(BETS)_2FeBr_4$. The sharp λ-type peak at 2.4 K and zero-magnetic field corresponds to AF transition. No anomaly was detected around T_c (≈1.1 K). By applying the magnetic field perpendicular to the conduction plane, the peak position shifts to lower temperature: 2.36 K at 1 T and 2.05 A at 2 T. The inset is the temperature dependence of the entropy (S), which reaches to R ln 6 (=R ln(2S + 1), $S = 5/2$) at about 3.8 K.

Furthermore, no distinct anomaly could be detected around 1.1 K, which demonstrates that the magnetically ordered state is not destroyed by the onset of superconducting transition. Therefore, it may be said that the specific heat also shows the coexistence of the magnetic order and the superconductivity below T_c. In the inorganic materials, the coexistence of the antiferromagnetic order and superconductivity has been found in the ternary systems such as the rhodium-boride phase, $RERh_4B_4$ (RE = Nd, Sm) and the so-called Chevrel compounds, $REMo_6S_8$ (RE = Gd, Tb, Dy, and Er) in which the 4d electrons of Rh or Mo atoms show superconductivity and the 4f spins of rare earth atoms antiferromagnetically order below the superconducting transition temperature.[101,102] However, the phase transition from the antiferromagnetic metal phase to the antiferromagnetic superconducting phase as is observed in the κ-$(BETS)_2FeBr_4$ salt is quite unusual, and only one system, $Ho(Ir_xRh_{1-x})_4B_4$ ($x \geq 0.6$), was reported to our knowledge.[103]

As mentioned before, unlike κ-$(BETS)_2FeBr_4$ with a broad resistivity peak around 60 K, κ-$(BETS)_2FeCl_4$ exhibits a normal metallic behavior down to very low temperature. Although the superconducting transition has not been observed by the resistivity measurements, the *ac* susceptibility and μSR experiments revealed κ-$(BETS)_2FeCl_4$ to be the second antiferromagnetic organic superconductor.[68,104] As shown in Figure 35, the *ac* susceptibility and specific heat measurements showed the antiferromagnetic transition at 0.45 K, which is about five times smaller than T_N of κ-$(BETS)_2FeBr_4$. The large susceptibility decrease below 0.15 K suggests the superconducting transition. Recently, Pratt et al. have performed μSR experiments, which provided unambiguous evidence for the coexistence of antiferromagnetic order and superconductivity blow T_c ($T_N = 0.45$ K and $T_c \approx 0.17$ K (see Figure 36)). The main precession signals were observed in the regions of 17−20 MHz (F1) and 1 MHz (F2). Unlike F1, the drop of the frequency was

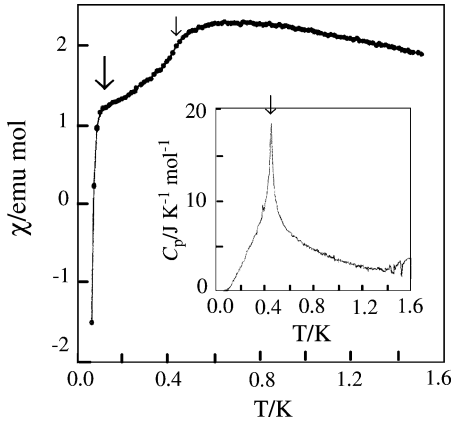

Figure 35. *ac* susceptibility of polycrystalline sample of κ-(BETS)$_2$FeCl$_4$. The arrows indicate the AF and SC transitions. The inset is the specific heat, indicating T_N to be 0.45 K. The peak of the specific heat trails a significant tail, indicating low dimensionality of the spin system.

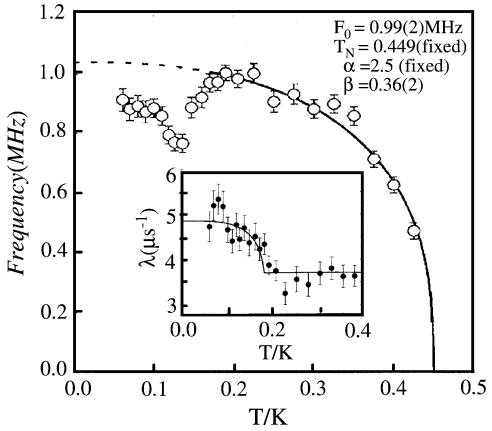

Figure 36. Temperature dependence of the low-frequency component in the 1 MHz region of μSR signal of κ-(BETS)$_2$FeCl$_4$: the inset is the damping rate.[104]

observed in F2 around 0.17 K, providing the evidence for the presence in the normal state of a weak SDW within the BETS layers, as theoretically suggested by Hotta and Fukuyama.[104,105]

A sharp peak of the specific heat observed at 0.45 K suggested the development of antiferromagnetic long-range order. However, no anomaly was detected around T_c (≈0.17 K), which also suggests the coexistence of the magnetic order and superconductivity below T_c. Furthermore, the peak of specific heat of κ-(BETS)$_2$FeCl$_4$ trails a significant tail at the temperature region higher than T_N. In fact, the entropy $S(T)$ around the T_N calculated by neglecting small contributions from the lattice and the conduction electrons shows a gradual increase at $T > T_N$ but reaches no more than ca. 86% of the expected total magnetic entropy $S_o = R \ln(2S + 1)$ (= 14.9 J/mol K for $S = 5/2$): at $T = 3T_N$ (≈1.35 K) S is $0.81S_o$. The magnetic entropy of κ-(BETS)$_2$FeCl$_4$ is $S(T_N) = 0.40S_o$, which is considerably smaller than the entropy of κ-(BETS)$_2$FeBr$_4$: $S = 0.64S_o$ at T_N and $1.0S_o$ at 3.6 K (≈1.5 T_N).[67,68]

In contrast to λ-type salt, where the crystals of λ-(BETS)$_2$FeBr$_x$Cl$_{4-x}$ are obtained only for small x-range ($x < 0.9$), Br and Cl atoms are exchanged freely in κ-type salts, κ-(BETS)$_2$FeBr$_x$Cl$_{4-x}$ ($0 \le x \le$

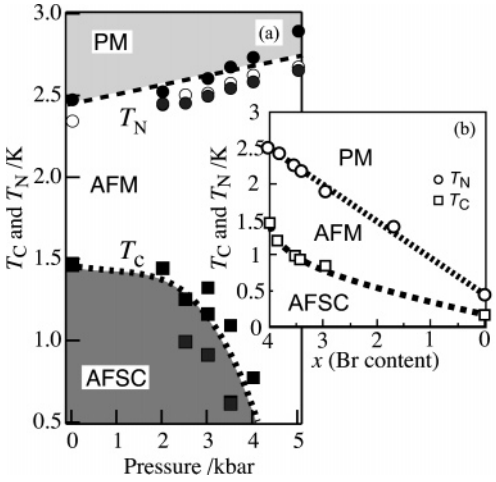

Figure 37. (a) Pressure−temperature phase diagram of κ-(BETS)$_2$FeBr$_4$. The circle and square denote the Néel temperature T_N and onset temperatures of resistivity drop T_C, respectively. (b) The composition−temperature phase diagram of κ-(BETS)$_2$FeBr$_x$Cl$_{4-x}$.

4). Therefore, the magnetic and superconducting properties of κ-type salt can be changed continuously in the wide range. As mentioned before, the susceptibility of κ-(BETS)$_2$FeBr$_x$Cl$_{4-x}$ ($x = 4.0$) for the field parallel to a [|| the easy axis of the antiferromagnetic spin structure] decreased with lowering temperature around 2 K. However, in the sample with $x < 2.4$, the susceptibility decrease was hardly observable above 2 K for the field parallel to the a axis, while the susceptibility decrease was observed for the field parallel to the b axis, indicating the rotation of easy axis from a to b with increasing Cl content. Similar rotation of the easy axis of spin structure by the halogen exchange has been found in the antiferromagnetic insulating state of λ-(BETS)$_2$FeBr$_x$Cl$_{4-x}$.[92] Both T_c and T_N decrease with increasing Cl content. Usually, Br/Cl exchange exerts the effective pressure (chemical pressure) on the π conduction electrons. In fact, we have recently confirmed the strong suppression of T_c of κ-(BETS)$_2$FeBr$_4$ around 3 kbar.[106] On the other hands, contrary to the Br/Cl exchange effect, T_N was increased with pressure. The pressure−temperature phase diagram of κ-(BETS)$_2$FeBr$_4$ and the composition−temperature phase diagram of κ-(BETS)$_2$FeBr$_x$Cl$_{4-x}$ are given in Figure 37.

4.4. Field-Induced Superconductivity and Switching Behavior of Electrical Properties of Magnetic Organic Superconductor

Recent discovery of the field-induced superconductivity in λ-(BETS)$_2$FeCl$_4$ at very high magnetic field has aroused considerable interest.[81] Jaccarino−Peter compensation of the external magnetic field in a 2-D superconductor is essential to realize such novel phenomena. As mentioned before, π electrons of λ-(BETS)$_2$MCl$_4$ (M = Ga, Fe) tend to take the superconducting state at low temperatures. But in FeCl$_4$ salt, the coupling between π metal electrons and 3d localized magnetic moments suppresses the superconducting transition to produce the π−d coupled antiferromagnetic insulating state. The superconducting state of λ-(BETS)$_2$FeCl$_4$ is realized by apply-

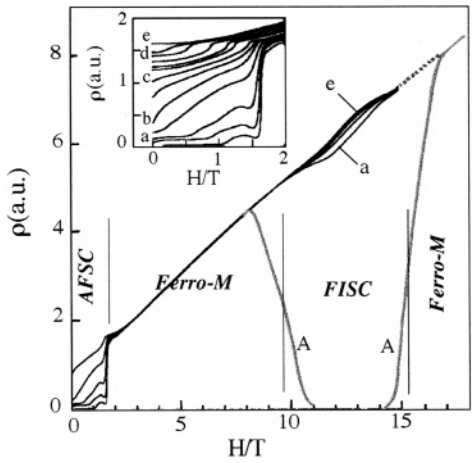

Figure 38. Magnetic field dependence of the resistivity up to 15 T and down to 0.58 K for the field approximately parallel to a: $a = 0.58$ K, $b = 1.04$, $c = 1.37$, $d = 2.34$, and $e = 2.55$ (the temperatures are increased from the lowest line (a) to the highest line (e), but the temperatures are not indicated to all the resistivity curves due to the limitation of the space). The resistivity data (A) up to 18 T at 27 mK were obtained by Konoike et al. where the magnetic field is exactly parallel to a.[108]

ing a high magnetic field where Fe^{3+} spins are forced to orient ferromagnetically or by applying high pressure where the MI transition and AF transition cannot be coupled. Similar compensation of the external field by the internal magnetic field through AF coupling between ferromagnetically oriented Fe^{3+} spins and π conduction electrons will be also expected in κ-$(BETS)_2FeBr_4$, which has an antiferromagnetic superconducting ground state at zero magnetic field. Since smaller $\pi-d$ interaction is suggested from the relatively weak intermolecular contacts, the compensation in κ-$(BETS)_2FeBr_4$ will be satisfied at a lower magnetic field.

The low-temperature resistivity measurements under magnetic field showed a very sharp resistivity increase at 1.6 T for $H\|a$ (Figure 38).[107] Of course, this corresponds to the transition from an antiferromagnetic superconducting state to a ferromagnetic metal state coupled with the metamagnetic transition. The magnetic field dependence of resistivities measured up to 15 T and down to 0.6 K showed distinct resistivity decreases at two magnetic fields: (1) a resistivity dip just before the large resistivity jump around 1.6 T and (2) a resistivity anomaly around 12.5 T.[107] This indicates that in κ-$(BETS)_2FeBr_4$, the compensation occurs at two magnetic field (H_{JP1} and H_{JP2}). Figure 39 illustrates the relationship between H_{eff} ($= H_{ext} - H_{int}$) and H_{ext}, where H_{int} and H_{ext} are the internal field produced by antiferromagnetic coupling between π electrons and ferromagnetically oriented Fe^{3+} moments and the external magnetic field, respectively, and H_{eff} is the effective magnetic field on BETS layer. Here, H_{int} may be assumed to be proportional to the magnetization of the Fe^{3+} spins. When applying the external magnetic field parallel to the easy axis ($H\|a$), the sign of $H_{eff}\|a$ is considered to be changed from positive to negative at 1.6 T (H_{JP1}) and then to return to positive at the field (H_{JP2}) corresponding to the internal field produced by the fully magnetized Fe^{3+} spin system. This

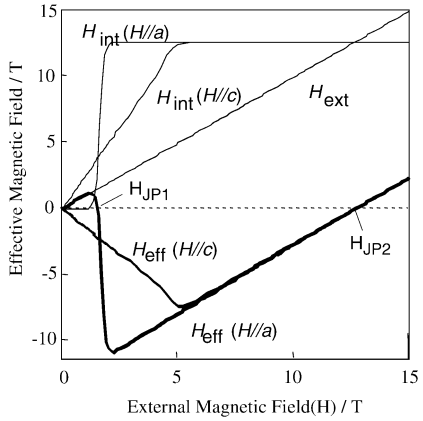

Figure 39. Schematic plot of applied external magnetic field (H_{ext}) dependence of the internal field (H_{int}) produced by Fe^{3+} moments in κ-$(BETS)_2FeBr_4$ and effective field (H_{eff}) on BETS layers, which is obtained as $H_{eff} = H_{ext} - H_{int}$. H_{JP1} and H_{JP2} indicate the fields where the Jaccarino–Peter compensation effect is satisfied.

is the reason there are two zero-field points at H_{JP1} and H_{JP2} ($H_{eff} = 0$). Recently, Konoike et al. have confirmed the FISC around 12.6 T.[108] On the other hand, on the application of the magnetic field parallel to the hard axis ($H\|c$), initial effective fields are already negative because of large magnetization of Fe^{3+} spins (Figure 39), and only one compensation point will be expected at H_{JP2} ($=H_o$), which is consistent with the result of the preliminary resistivity measurements down to 0.6 K showing the resistivity decrease around 12.5 T also for $H\|c$.[108]

The critical field of this field-induced superconducting state ($H_{JP2} \approx 12.5$ T) is about one-third of that of the first magnetic-field-induced organic superconductor λ-$(BETS)_2FeCl_4$ ($H_{JP} = 33$ T). These two salts have several resemblances: they have the layered structure consisting of the two-dimensional conducting layers and the insulating layers involving the magnetic iron atoms with $S = 5/2$, which show the antiferromagnetic transition at low temperatures. But their ground states are quite different. In the λ-$(BETS)_2FeCl_4$ salt, the strong $\pi-d$ coupling between the BETS semi-cations and the $FeCl_4^-$ anions suggested from many short contacts between Cl and chalcogen atoms resulted in the cooperative transition to the antiferromagnetic insulating state at T_N. On the other hand, such short intermolecular contacts were not observed in κ-$(BETS)_2FeBr_4$, and consequently, the metallic state could be maintained during the antiferromagnetic transition of the anion layers, and the antiferromagnetic superconducting state was realized. Therefore, the induced internal magnetic field on the BETS layers in κ-$(BETS)_2FeBr_4$ is considered to be weaker than that in λ-$(BETS)_2FeCl_4$, which is consistent with the smaller compensation field of κ-$(BETS)_2FeBr_4$. However, for $H\|a$, the situation of κ-$(BETS)_2FeBr_4$ is more complicated because of the existence of the metamagnetic transition, which makes this system a dual functional material and gives rise to the field-induced resistivity decreases suggesting the stabilization of the superconducting state at two characteristic magnetic fields of 1.6 and 12.5 T.

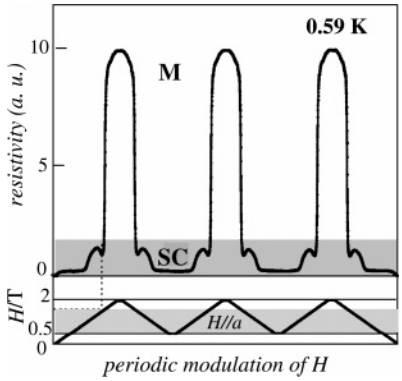

Figure 40. Switching behavior observed in κ-$(BETS)_2FeBr_4$. The periodic superconductor−metal switching associated with the periodical modulation of magnetic field ($H \| a$) around 1.6 T at 0.59 K. Unlike the usual superconductor destroyed by external field, the superconductivity is broken by the internal magnetic field produced by metamagnetic transition.

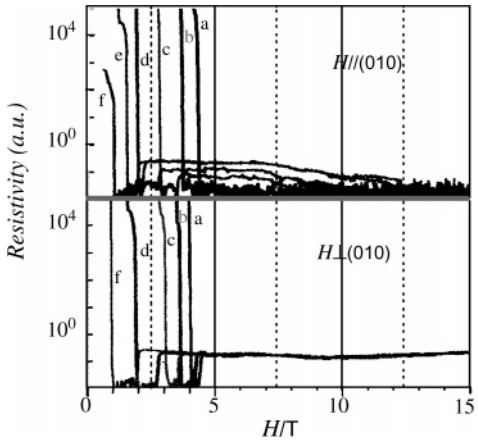

Figure 41. Magnetoresistance of λ-$(BETS)_2Fe_{0.4}Ga_{0.6}Cl_4$ up to 15 K at 1.6−3.4 K for the magnetic field parallel (upper part) and perpendicular (lower part) to the *ac* conduction plane: $a = 1.6$, $b = 2.0$, $c = 2.5$, $d = 3.0$, $e = 3.3$, and $f = 3.4$ K.

It is crucial to realize the molecular devices, to develop the molecular systems whose conducting properties can be widely controlled by external forces. Because of the interplay of π and d electrons, the conducting properties of κ-$(BETS)_2FeBr_4$ can be sharply switched between superconducting state and metallic state by changing the external field around 1.6 T at low temperatures (Figure 40).[109] More unique switching behavior can be observed in λ-$(BETS)_2Fe_xGa_{1-x}Cl_4$ ($x \approx 0.4$) exhibiting an unprecedented superconductor-to-insulator transition. We have made the magnetoresistance experiments at 1.6−3.4 K (Figure 41). When the magnetic field was applied perpendicular to the *ac* conduction plane, successive insulator → superconductor → metal transitions were observed with increasing the magnetic field. There exists a very narrow superconducting region between AF insulting phase and forced ferromagnetic metal phase. Also, for the field parallel to the *ac* plane, unprecedented resistivity behavior could be seen. Below 2 K, the insulator → superconductor transition was observed at 3.5−6 T. While above 2.5 K, the insulator → superconductor → metal → superconductor (→ metal) transitions took place successively with

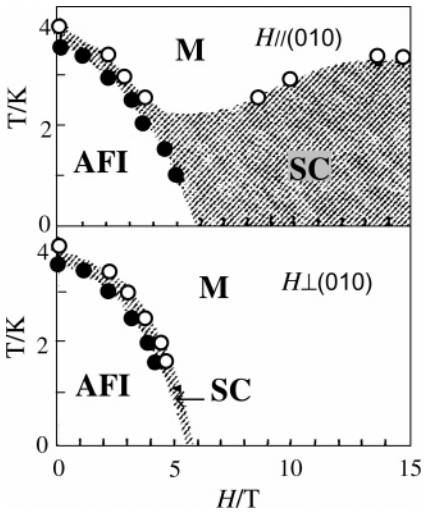

Figure 42. Temperature vs magnetic field phase diagram of λ-$(BETS)_2Fe_{0.4}Ga_{0.6}Cl_4$ for the field parallel (upper part) and perpendicular (lower part) to the conduction plane. The open and closed circles indicate metal-to-superconductor and superconductor-to-insulator transition temperatures, respectively: AFI = antiferromagnetic insulating phase, M = metal, and SC = superconductor.

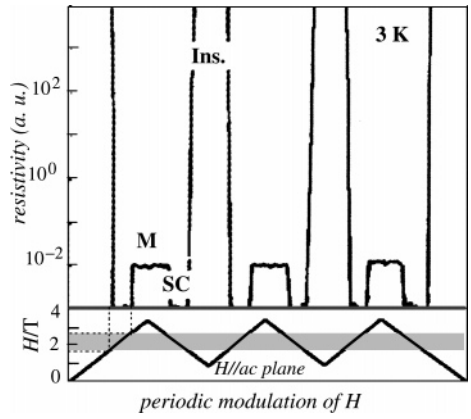

Figure 43. Example of switching behavior of the resistivity of λ-$(BETS)_2Fe_{0.4}Ga_{0.6}Cl_4$. The insulator−superconductor-−metal switching behavior was realized by the periodic modulation of magnetic field around 2.5 T ($H \| ac$ plane) at 3 K.

increasing the magnetic field (the last superconductor → metal transition will be observed above 15 T). The lower-field superconducting phase is considered to be the same superconducting phase as that observed for the field perpendicular to the conduction plane, while the high-field superconducting phase around 14 T observed only for the field parallel to the conduction plane corresponds to the FISC phase (Figure 41). It will be natural that the FISC phase of λ-$(BETS)_2Fe_{0.4}Ga_{0.6}Cl_4$ appears around 14 T because the density of magnetic moments of Fe^{3+} is 40% of pure $FeCl_4$ salt with FISC phase around 33T (33 T × 0.4 ≈ 13 T). Owing to the unique phase diagram (Figure 42), the periodic insulator → superconductor → metal changes could be realized in a stepwise manner by the periodic modulation of the external field (Figure 43). To our knowledge, this is the first conducting system whose insulating, metallic, and superconducting state can be selectively realized by slightly tuning the external field, although such switching phenomena are realized only at low temperatures. If a new

superconductor with similar phase diagram at high temperature can be developed, it will provide a clue as to how to realize a molecular switching device based on the interplay between localized magnetic moments and conduction elections.

5. Conclusions

Until the beginning of 1990s, there was no example of magnetic molecular conductors in which π metal-like conduction electrons and magnetic moments coexisted at low temperature. Therefore, the development of unprecedented magnetic organic metals and superconductors with novel electromagnetic properties produced by the interplay between π conduction electrons of organic layers and localized magnetic moments of the inorganic anion layers became one of the main targets in the field of chemistry of molecular conductors. The discoveries of a paramagnetic organic superconductor reported by P. Day et al.[27] and a ferromagnetic metal by Coronado et al.[28] are well-known achievements. When using BETS molecules and typical magnetic anions such as $FeCl_4^-$ and $FeBr_4^-$, various types of new magnetic conductors including the first antiferromagnetic and metamagnetic organic metals and antiferromagnetic organic superconductors have been discovered. In addition, the existence of considerable $\pi-$d interactions in magnetic organic metals has been proved. Furthermore, the conductors exhibiting unprecedented superconductor−insulator transitions and field-induced organic superconductors have been also disclosed.

Since the molecules tend to retain their individualities even in the solid state, it might be imagined that it is not so difficult to construct multifunctional systems by assembling various molecular building blocks with different characters. In fact, we have discovered new types of molecular superconductors whose conducting properties can be sharply switched by slightly tuning the external magnetic field.

One of the next targets in the development of new magnetic molecular conductors may be the development of new conductors usable for the molecular spintronics. To prepare the organic conductors with sufficiently large spin polarization of π metal electrons, the strong $\pi-$d interaction will be needed. At first sight, the $\pi-$d interaction in an organic/inorganic hybrid system composed of conducting π donor layers and magnetic anion layer seems to be fairly small because direct overlap of the 3d orbital of magnetic transition metal ions and HOMO of π molecules cannot be expected. However, the field-induced superconductivity of λ-$(BETS)_2FeCl_4$ has reveled that the $\pi-$d interaction can produce the effective magnetic field higher than 30 T. Therefore, it might be possible in the future to obtain the organic conductor with sufficiently large spin polarization at fairly high temperatures.

Although the organic superconductor with a 3-D antiferromagnetic order has been discovered, the ferromagnetic organic superconductor has not been discovered yet. In inorganic systems, a few ferromagnetic superconductors such as UGe_2, $ZrZn_2$, and $RuSr_2GdCu_2O_8$ have been reported.[110−112] In general, the superconductivity and ferromagnetism is not compatible. However, $RuSr_2GdCu_2O_8$ with a layered structure similar to the 2-D organic superconductor has a fairly high transition temperatures of T_C (Curie temperature = 133 K) and T_c (superconducting temperature = 12−24 K), where the authors suggested the possibility of a large enhancement of T_c (up to 40 K) by annealing the sample.[112] Therefore, it will be possible to prepare a layered ferromagnetic organic superconductor composed of π donor layers and inorganic anion layers.

6. Acknowledgments

This paper is mainly based on recent works made in collaboration with Drs. H. Tanaka, A. Akutsu, H. Akutsu, E. Fujiwara, H. Fujiwara, Zhang Bin, M. Tokumoto, P. Cassoux, S. Uji, and Prof. Brooks. The authors express their thanks to all of them. We are indebted to CREST (Core Research for Evolutional Science and Technology) of JST (Japan Science and Technology Corp.) for financial support. This study was also supported by a Grant-in-Aid for Scientific Research on (*S*) (14103005), Priority Areas of Molecular Conductors (15073209), and for the 21st Century COE Program for Frontiers in Fundamental Chemistry from the Ministry of Education, Culture, Sports, Science and Technology.

7. References

(1) Jérome, D.; Mazaud, D.; Ribault, M.; Bechgaard, K. *J. Phys. Lett.* **1980**, *L95*, 1416.
(2) Bechgaard, K.; Jacobsen, C. S.; Mortensen, M.; Pedersen, H. J.; Thorup, N. *Solid State Commun*. **1980**, *33*, 1119.
(3) Thorup, N.; Rindorf, G.; Soling, H.; Bechgaard, K. *Acta Cryst*. **1981**, *B37*, 1236.
(4) For example, see Mori, T.; Kobayashi, A.; Sasaki, Y.; Kobayashi, H. *Chem. Lett*. **1982**, 1923.
(5) (a) Yagubskii, E. B.; Shchegolev, I. F.; Laukhin, V. N.; Kononovich, P. A.; Kartsovnik, M. V.; Zvarykina, A. V.; Buravov, L. I. *JETP Lett*. **1984**, *39*, 12. (b) Kobayashi, A.; Kato, R.; Kobayashi, H.; Moriyama, H.; Nishio, Y.; Kajita, K.; Sasaki W. *Chem. Lett*. **1987**, 459. (c) Urayama, H.; Yamochi, H.; Saito, G.; Kawamoto, A.; Tanaka, J.; Mori, T.; Maruyama, Y.; Inokuchi, H. *Chem. Lett*. **1988**, 463.
(6) Williams, J. M.; Ferraro, J. R.; Thorn, R. J.; Carlson, K. D.; Geiser, U.; Wang, H. H.; Kini, A. M.; Whangbo, M.-H. *Organic Superconductors (Including Fullerene)*; Prentice Hall: Englewood Cliffs, NJ, 1992, and references therein.
(7) (a) Oshima, K.; Mori, T.; Inokuchi, H.; Urayama, H.; Yamochi, H.; Saito, G. *Phys. Rev*. **1988**, *B38*, 938. (b) Kang, W.; Montambaux, G.; Cooper, J. R.; Jerome, D.; Batail, P.; Lenoir, C. *Phys. Rev. Lett*. **1989**, *62*, 2559.
(8) (a) Brossard, L.; Ribault, M.; Valade, L.; Cassoux, P. *Physica* **1986**, *B143*, 378. (b) Kobayashi, A.; Kim, H.; Sasaki, Y.; Kato, R.; Kobayashi, H.; Moriyama, S.; Nishio, Y.; Kajita, K.; Sasaki, W. *Chem. Lett*. **1987**, 1819. (c) Cassoux, P.; Valade, L.; Kobayashi, H.; Kobayashi, A.; Clark, R. A.; Underhill, A. E. *Coord. Chem. Rev*. **1991**, *110*, 115. (d) Tajima, H.; Inokuchi, M.; Kobayashi, A.; Ohta, T.; Kato, R.; Kobayashi, H.; Kuroda, H. *Chem. Lett*. **1993**, 1235.
(9) Bednorz, J. G.; Müller, K. A. *Zitschrift Phys*. **1986**, *B64*, 189.
(10) Aumüller, A.; Erk, P.; Klebe, G.; Hünig, S.; von Schutz, J. U.; Werner, H.-P. *Angew. Chem., Int. Ed. Engl*. **1986**, *25*, 740.
(11) Kobayashi, A.; Kato, R.; Kobayashi, H.; Mori, T.; Inokuchi, H. *Solid State Commun*. **1987**, *64*, 45.
(12) Inoue, I. H.; Kakizaki, A.; Namatame, H.; Fujimori, A.; Kobayashi, A.; Kato, R.; Kobayashi, H. *Phys. Rev*. **1992**, *B45*, 5828.
(13) Uji, S.; Terashima, T.; Aoki, H.; Brooks, J. S.; Kato, R.; Sawa, H.; Aonuma, S.; Tamura, M.; Kinoshita, M. *Phys. Rev*. **1994**, *B50*, 15597.
(14) Miyazaki, T.; Terakura, K.; Morikawa, Y.; Yamasaki, T. *Phys. Rev. Lett*. **1995**, *74*, 5104.
(15) (a) Kobayashi, H.; Miyamoto, A.; Kato, R.; Sasaki, F.; Kobayashi, A.; Yamakita, Y.; Furukawa, Y.; Tasumi, M.; Watanabe, T. *Phys. Rev*. **1993**, *B47*, 3500. (b) Kato, R.; Kobayashi, H.; Kobayashi, A. *J. Am. Chem. Soc*. **1989**, *111*, 5224.

(16) (a) Ogawa, M. Y.; Palmer, S. M.; Liou, K. K.; Quirion, G.; Thompson, J. A.; Poirier, M.; Hoffman, B. *Phys. Rev*. **1989**, *B39*, 10682. (b) Quirion, G.; Poier, M.; Liou, K. K.; Hoffman, B. *Phys. Rev*. **1991**, *B43*, 860.

(17) (a) Hanasaki, N.; Tajima, H.; Matsuda, M.; Naito, T.; Inabe, T. *Phys. Rev*. **2000**, *B6*, 5839. (b) Matsuda, M.; Naito, T.; Inabe, I.; Hanazaki, N.; Tajima, H.; Otsuka, T.; Awaga, K.; Narymbetov, B.; Kobayashi, H. *J. Mater. Chem*. **2000**, *10*, 631.

(18) Almeida, M.; Henriques, R. In *Handbook of Organic Conductive Molecules and Polymer*; Nalwa, H. S., Ed.; J. Wiley: New York, 1997; Vol. 1, pp 87−149, and references therein.

(19) Ribera, E.; Rovira, C.; Veciana, J.; Tarres, J.; Canadell, E.; Rousseau, R.; Molins, E.; Mas, M.; Schoeffel, J.-P.; Pouget, J.-P.; Morgado, J.; Henriques, R. T.; Almeida, M. *Chem.—Eur. J*. **1999**, *5*, 2025.

(20) Imai, H.; Otsuka, T.; Naito, T.; Awaga, K.; Inabe, T. *J. Am. Chem. Soc*. **1999**, *121*, 8098.

(21) Dagotto, E.; Riera J.; Scalapino, D. *Phys. Rev*. **1992**, *B45*, 5744.

(22) Nakazaki, J.; Chung, I.; Mstsushita, M. M.; Sugawara, T.; Watanabe, R.; Izuoka, A.; Kawada, Y. *J. Mater. Chem*. **2003**, *13*, 1011.

(23) Mukai, K.; Jinno, S.; Shimobe, Y.; Azuma, N.; Taniguchi, M.; Misaki, Y.; Tanaka, K.; Inoue K.; Hosokoshi, Y. *J. Mater. Chem*. **2003**, *13*, 1614.

(24) Tanaka, H.; Okano, Y.; Kobayashi, H.; Suzuki, W.; Kobayashi, A. *Science* **2001**, *291*, 285.

(25) Kobayashi, A.; Tanaka, H.; Kobayashi, H. *J. Mater. Chem.* **2001**, *11*, 2078.

(26) Fujiwara, H.; Lee, H.; Cui, H.; Kobayashi, H.; Fujiwara, E.; Kobayashi, A. *Adv. Mater*., in press.

(27) (a) Kurmoo, M.; Graham, A. W.; Day, P.; Coles, S. J.; Hursthouse, M. B.; Caulfield, J. L.; Singleton, J.; Pratt, F. L.; Hayes, W.; Ducasse, L.; Guionneau, P. *J. Am. Chem. Soc.* **1995**, *117*, 12209. (b) Martin, L.; Turner, S. S.; Day, P.; Guionneau, P.; Howard, J. A. K.; Hidds, D. E.; Light, M. E.; Hursthouse, M. B.; Uruichi, M.; Yakushi, K. *Inorg. Chem*. **2001**, *40*, 1363.

(28) Coronado, E.; Galan-Mascaros, J. R.; Gomez-Garcia, C. J.; Laukhin, V. *Nature* **2000**, *408*, 447.

(29) Tamaki, H.; Zhong, Z. J.; Matsumoto, N.; Kida, S.; Koikawa, M.; Achiwa, N.; Hashimoto, Y.; Okawa, H. *J. Am. Chem. Soc*. **1992**, *114*, 6974.

(30) Suzuki, W.; Fujiwara, E.; Kobayashi, A.; Fujishiro, Y.; Nishibori, E.; Takata, M.; Sakata, M.; Fujiwara, H.; Kobayashi, H. *J. Am. Chem. Soc.* **2003**, *125*, 1486.

(31) Palacio, F.; Miller, J. S. *Nature* **2000**, *408*, 421.

(32) Kobayashi, A.; Udagawa, T.; Tomita, H.; Naito, T.; Kobayashi, H. *Chem. Lett*. **1993**, 2179.

(33) Schumaker, R. P.; Lee, V. Y.; Engler, E. M. *IBM Res. Rep.* **1983**.

(34) (a) Kato, R.; Kobayashi, H.; Kobayashi, A. *Synth. Met.* **1991**, *41*−*43*, 2093, and references therein. (b) Kato, R.; Kobayashi, H.; Kobayashi, A. *Chem. Lett*. **1991**, 1045. (c) Fujiwara, M.; Tajima, N.; Imakubo, T.; Tamura, M.; Kato, R. *J. Solid State Chem*. **2002**, *168*, 396.

(35) Courcet, T.; Malfant, I.; Cassoux, P. *New J. Chem.* **1998**, 585, and references therein.

(36) Takimiya, K.; Kataoka, Y.; Niihara, N.; Aso, Y.; Otsubo, T. *J. Org. Chem*. **2003**, *68*, 5217.

(37) Tanaka, H.; Kobayashi, A.; Sato, A.; Akutsu, H.; Kobayashi, H. *J. Am. Chem. Soc.* **1999**, *121*, 760.

(38) Kobayashi, A.; Kato, R.; Kobayashi, H. *Synth. Met*. **1993**, *55*−*57*, 2078.

(39) Naito, T.; Miyamoto, A.; Kobayashi, H.; Kato, R.; Kobayashi, A. *Chem. Lett.* **1991**, 1945.

(40) Gritsenko, V.; Tanaka, H.; Kobayashi, H.; Kobayashi, A. *J. Mater. Chem*. **2001**, *11*, 2410.

(41) Montgomery, L. K.; Burgin, T.; Huffman, J. C.; Carlson, K. D.; Dudek, J. D.; Yaconi, G. A.; Megna, L. A.; Mobley, P. R.; Kwok, W. K.; Williams, J. M.; Schirber, J. E.; Overmyer, D. I.; Ren, J.; Rovira, C.; Whangbo, M.-H. *Synth. Met*. **1993**, *55*−*57*, 2090.

(42) Montgomery, L. K.; Fravel, B. W.; Huffman, J. C.; Agosta, C.; Ivanov, S. A. *Synth. Met.* **1997**, *85*, 1621.

(43) Narymbetov, B. Z.; Kushch, N.; Zorin, L. V.; Khasanov, S. S.; Shibaeva, R. P.; Togonidze, T. G.; Kovalev, A. E.; Kartsovnik, M. V.; Buravov, L. I.; Yagubskii, E. B.; Canadell, E.; Kobayashi, A.; Kobayashi, H. *Eur. Phys. J*. **1998**, *5*, 179.

(44) Cassoux, P.; Faulmann, C.; Garreau de Bonneval, B.; Malfant, I.; Aonuma, S.; Sanchez, M. E. *Synth. Met.* **2001**, *120*, 1085.

(45) Sanchez, M. D.; Doublet, M. L.; Faulmann, C.; Malfant, I.; Cassoux, P.; Kushch, N. D.; Yagubskii, E. B. *Eur. J. Inorg. Chem.* **2001**, 2797.

(46) Fujiwara, E.; Gritsenko, V.; Fujiwara, H.; Tamura, I.; Kobayashi, H.; Tokumoto, M.; Kobayashi, A. *Inorg. Chem*. **2002**, *41*, 3230.

(47) Gritsenko, V.; Fujiwara, E.; Fujiwara, H.; Kobyashi, H. *Synth. Met.* **2002**, *128*, 273.

(48) Kobayashi, A.; Sato, A.; Arai, E.; Kobayashi, H.; Faulmann, C.; Kushch N.; Cassoux, P. *Solid State Commun*. **1997**, *103*, 371.

(49) Kushch, N. D.; Dyachenko, O. A.; Gritsenko, V. V.; Buravov, L. I.; Tkacheva, V. A.; Yagubskii, E. B.; Kaplunov, M. G.; Golubrv, E. N.; Togonide, T. G.; Kobayashi, A.; Kobayashi, H. *J. Mater. Chem*. **1999**, *9*, 687.

(50) Kushch, N. D.; Dyachenko, O. A.; Gritsenko, V. V.; Cassoux, P.; Faulmann, C.; Kobayashi, A.; Kobayashi, H. *J. Chem. Soc., Dalton Trans.* **1998**, 683.

(51) Kushch, N. D.; Buravov, L. I.; Pesotskii, S. I.; Lyubovskii, R. B.; Yagubskii, E. B.; Kaplunov, M. G.; Golubev, E. V.; Narymbetov, B. Z.; Khasanov, S. S.; Zorina, L. V.; Rozenberg, L.; Shibaeva, R.; Kobayashi, A.; Kobayashi, H. *J. Mater. Chem*. **1998**, *8*, 897.

(52) Kobayashi, A.; Kobayashi, H. *Mol. Cryst. Liq. Cryst.* **1997**, *296*, 181.

(53) Tanaka, H.; Kobayashi, A.; Kobayashi, H. *Bull. Chem. Soc. Jpn.* **1997**, *70*, 3137.

(54) Alberola, A.; Coronado, E.; Galan-Mascaros, J. R.; Gimenez-Zaiz, C.; Gomez-Garcia, C. J. *J. Am. Chem. Soc*. **2003**, *125*, 10774.

(55) Cui, H.; Zhang, B.; Kobayashi, H.; Kobayashi, A., to be submitted.

(56) Kondo, R.; Hasegawa, T.; Mochida, T.; Kagoshima, S.; Iwasa, Y. *Chem. Lett.* **1999**, 333.

(57) Tanaka, H.; Kobayashi, A.; Sato, A.; Akutsu, H.; Kobayashi, H. *J. Am. Chem. Soc*. **1999**, *121*, 760.

(58) Kobayashi, H.; Tomita, H.; Kobayashi, A.; Sakai, F.; Watanabe, T.; Cassoux, P. *J. Am. Chem. Soc.* **1996**, *118*, 368.

(59) Tanaka, H.; Kobayashi, A.; Kobayashi, H. *Chem. Lett.* **1999**, 133.

(60) Kondo, R.; Hasegawa, T.; Mochida, T.; Kagoshima, S.; Iwasa, Y.; Hiraki, K.; Takahashi, T. *J. Phys. Soc. Jpn.* **2001**, *70*, 3023.

(61) Uji, S.; Shinagawa, H.; Terakura, C.; Terashima, T.; Yakabe, T.; Terai, Y.; Tokumoto, M.; Kobayashi, A.; Tanaka, H.; Kobayashi, H. *Phys. Rev.* **2001**, *B64*, 024531.

(62) Kobayashi, H.; Akutsu, H.; Arai, E.; Tanaka, H.; Kobayashi, A. *Phys. Rev*. **1997**, *B56*, R8526.

(63) Seo, H.; Fukuyama, H. *J. Phys. Soc. Jpn*. **1997**, *66*, 3352; *Synth. Met.* **1999**, *103*, 1951; Seo, H.; Hotta, C.; Fukuyama, H. *Chem. Rev.* **2004**, *104*, 5005.

(64) Tajima, H.; Kobayashi, A.; Naito, T.; Kobayashi, H. *Synth. Met*. **1997**, *86*, 1911.

(65) Konoike, T.; Fujiwara, H.; Zhang, B.; Kobayashi, H.; Nishimira, M.; Yasuzuka, S.; Enomoto, K.; Uji, S. *J. Phys. IV* **2004**, *114*, 223.

(66) Ojima, E.; Fujiwara, H.; Kato, K.; Kobayashi, H.; Tanaka, H.; Kobayashi, A.; Tokumoto, M.; Cassoux, P. *J. Am. Chem. Soc.* **1999**, *121*, 5581.

(67) Fujiwara, H.; Ojima, E.; Nakazawa, Y.; Narymbetov, Z. B.; Kato, K.; Kobayashi, H.; Kobayashi, A.; Tokumoto, M.; Cassoux, P. *J. Am. Chem. Soc*. **2001**, *123*, 306.

(68) Otsuka, T.; Kobayashi, A.; Miyamoto, Y.; Kiuchi, J.; Nakamura, S.; Wada, N.; Fujiwara, E.; Fujiwara, H.; Kobayashi, H. *J. Solid State Chem*. **2001**, *159*, 407.

(69) Tanaka, H.; Ojima, E.; Fujiwara, H.; Nakazawa, Y.; Kobayashi, H.; Kobayashi, A. *J. Mater. Chem.* **2000**, *10*, 245.

(70) Kini, A. M.; Geiser, U.; Wang, H. H.; Carlson, K. D.; Williams, J. M.; Kwok, W. K.; Vandervoort, K. G.; Thompson, J. E.; Stupka, D. L.; Jung, D.; Whangboo, M. H. *Inorg. Chem*. **1990**, *29*, 2555.

(71) Sakata, J.; Sato, H.; Miyazaki, A.; Enoki, T.; Okano, Y.; Kato, R. *Solid State Commun*. **1998**, *108*, 377.

(72) Matsui, H.; Tsuchiya, H.; Suzuki, T.; Negishi, E.; Toyota, N. *Phys. Rev*. **2003**, B *68*, 155105.

(73) Toyota, N.; Abe, Y.; Kuwabara, T.; Negishi E.; Matsui, H. *J. Phys. Soc. Jpn*. **2003**, *72*, 2714.

(74) Tokumoto, M.; Naito, T.; Kobayashi, H.; Kobayashi, A.; Laulhin, V. N.; Brossard, L.; Cassoux, P. *Synth. Met*. **1997**, *86*, 2161.

(75) Sasaki, T.; Uozaki, H.; Endo, S.; Toyota, N. *Synth. Met*. **2001**, *120*, 759.

(76) Recent magnetization torque experiments on λ-$(BETS)_2FeCl_4$ by Tanaka, H., et al. gave the angle between the *c* axis and the AF easy axis little larger than the angle (about 30°) first suggested by Sasaki et al. (ref 75).

(77) Akutsu, H.; Arai, E.; Kobayashi, H.; Tanaka, H.; Kobayashi, A.; Cassoux, P. *J. Am. Chem. Soc.* **1997**, *119*, 12681.

(78) Brossard, L.; Clerac, R.; Coulon, C.; Tokumoto, M.; Ziman, T.; Petrov, D. K.; Laukhin, V. N.; Naughton, M. J.; Audouard, A.; Goze, F.; Kobayashi, A.; Kobayashi, H.; Cassoux, P. *Eur. Phys. J.* **1998**, *B1*, 439.

(79) For example, see Tokura, Y.; Nagaosa, N. *Science* **2000**, *288,* 462.

(80) Tanaka, H.; Adachi, T.; Ojima, E.; Fujiwara, H.; Kato, K.; Kobayashi, H.; Kobayashi, A.; Cassoux, P. *J. Am. Chem. Soc*. 1999, *121*, 11243.

(81) Uji, S.; Shinagawa, H.; Terashima, T.; Yakabe, T.; Terai, Y.; Tokumoto, M.; Kobayashi, A.; Tanaka, H.; Kobayashi, H. *Nature* **2001**, *410*, 908.

(82) Balicas, L.; Brooks, J. S.; Storr, K.; Uji, S.; Tokumoto, M.; Tanaka, H.; Kobayashi, H.; Kobayashi, A.; Barzykin, V.; Go_kov, L. P. *Phys. Rev. Lett*. **2001**, *87*, 67002.

(83) Meul, H. W.; Rossel, C.; Decroux, M.; Fisher, F.; Remenyi, G.; Briggs, A. *Phys. Rev. Lett*. **1984**, *53*, 497.

(84) Jaccarino, V.; Peter, M. *Phys. Rev. Lett*. **1962**, *9*, 290.

(85) Uji, S.; Kobayashi, H.; Brooks, J. S. *Adv. Mater*. **2002**, *14*, 243.

(86) Cépas, O.; McKenzie, R. H.; Merino, J. *Phys. Rev*. **2002**, *B65*, 100502.
(87) Uji, S.; Shinagawa, H.; Terashima, T.; Terakura, C.; Yakabe, T.; Terai, Y.; Tokumoto, M.; Kobayashi, A.; Tanaka, H.; Kobayashi, H. *Phys. Rev.* **2001**, *B64*, 24531.
(88) Tanatar, M. A.; Ishiguro, T.; Tanaka, H.; Kobayashi, A.; Kobayashi, H. *J. Supercond*. **1999**, *12*, 511.
(89) Tanatar, M. A.; Ishiguro, T.; Tanaka, H.; Kobayashi, H. *Phys. Rev*. **2002**, *B66*, 134503.
(90) Shimahara, H. *J. Phys. Soc. Jpn.* **2002**, *71*, 1644.
(91) Houzet, M.; Buzdin, A.; Bulaevskii, L.; Maley, M. *Phys. Rev. Lett*. **2002**, *88*, 227001.
(92) Akutsu, H.; Kato, K.; Ojima, E.; Kobayashi, H.; Tanaka, H.; Kobayashi, A.; Cassoux, P. *Phys. Rev*. **1998**, *B58*, 9294.
(93) Uji, S.; Yasuzuka, S.; Tanaka, H.; Tokumoto, M.; Zhang, B.; Kobayashi, H.; Choi, E. S.; Graf, D.; Brooks, J. S. *J. Phys. IV France* **2004**, *114*, 391.
(94) Tokumoto, M.; Anzai, H.; Murata, K.; Kajimura, K.; Ishiguro, T. *Synth. Met*. **1988**, *27*, A251.
(95) When the superconducting transition of λ-$(BETS)_2Fe_xGa_{1-x}Cl_4$ ($x \approx 0.5$) was discovered in 1994, the superconducting state in the organic alloy system with such a high density of $FeCl_4$ anions seemed to be hardly acceptable for many people. But the discovery of the first paramagnetic organic superconductor by Kurmoo et al. (ref 27) in 1995 has wiped out such doubt completely.
(96) Kobayashi, H.; Sato, A.; Arai, E.; Akutsu, H.; Kobayashi, A.; Cassoux, P. *J. Am. Chem. Soc*. **1997**, *119*, 12392.
(97) Kobayashi, H.; Kobayashi, A.; Cassoux, P. *Chem. Soc. Rev*. **2000**, *29*, 325.
(98) Uji, S.; Shinagawa, H.; Terai, Y.; Yakabe, T.; Terakura, C.; Terashima, T.; Balicas, L.; Brooks, J. S.; Ojima, E.; Fujiwara, H.; Kobayashi, H.; Kobayashi, A.; Tokumoto, M. *Physica* **2001**, *B298*, 557, and references therein.
(99) Balicas, L.; Brooks, J. S.; Storr, K.; Graf, D.; Uji, S.; Shinagawa, H.; Ojima, F.; Fujiwara, H.; Kobayashi, H.; Kobayashi, A.; Tokumoto, M. *Solid State Commun*. **2000**, *116*, 557.
(100) Mori, T.; Katsuhara, M. *J. Phys. Soc. Jpn*. **2002**, *71*, 826.
(101) (a) Matthias, B. T.; Corenzwit, E.; Vandenberg, J. M.; Barz, H. E. *Proc. Natl. Acad. Sci. U.S.A.* **1977**, *74*, 1334. (b) Vandenberg, J. M.; Matthias, B. T. *Proc. Natl. Acad. Sci. U.S.A.* **1977**, *74*, 1336. (c) Matsumoto, H.; Umezawa, H. *Cryogenics* **1983**, 37.
(102) (a) Chevrel, R.; Sergent, M.; Prigent, J. *J. Solid State Chem.* **1971**, *3*, 515. (b) Fischer, Ø. *Appl. Phys.* **1978**, *16*, 1. (c) Ishikawa, M.; Fischer, Ø.; Muller, J. *J. Phys.* **1978**, *C6*, 1379. (d) Fischer, Ø.; Ishikawa, M.; Pelizzone, M.; Treyvaud, A. *J. Phys.* **1979**, *C5*, 89.
(103) Ku, H. C.; Acker, F.; Matthias, B. T. *Phys. Lett.* **1980**, *76A*, 399.
(104) Pratt, F. L.; Lee, S. I.; Blundell, S. J.; Marshall, I. M.; Uozaki, H.; Toyota, N. *Synth. Met*. **2003**, *133*−*134*, 489.
(105) Hotta, C.; Fukuyama, H. *J. Phys. Soc. Jpn*. **2000**, *69*, 2577.
(106) Otsuka, T.; Cui, H.; Fujiwara, H.; Kobayashi, H.; Fujiwara, E.; Kobayashi, A. J. *Mater. Chem*. **2004**, *14*, 1682.
(107) Fujiwara, H.; Kobayashi, H.; Fujiwara, E.; Kobayashi, A. *J. Am. Chem. Soc.* **2002**, *124*, 6816.
(108) Konoike, T.; Fujiwara, H.; Zhang, B.; Kobayashi, H.; Nishimura, M.; Yasuzuka, S.; Enomoto, K.; Uji, S. *J. Phys*. **2004**, *114*, 223.
(109) Zhang, B.; Tanaka, H.; Fujiwara, H.; Kobayashi, H.; Fujiwara, E.; Kobayashi, A. *J. Am. Chem. Soc.* **2002**, *124*, 9982.
(110) Saxena, S. S.; Agarwal, P.; Ahllan, K.; Grosche, F. M.; Haselwimmer, R. K. W.; Steiner, M. J.; Pugh, E.; Walker, I. R.; Jullan, S. R.; Monthoux, P.; Lonzarich, G. G.; Huxley, A.; Shelkin, I.; Braithwalte, D.; Flouquet, J. *Nature* **2000**, *406*, 587.
(111) Pfleider, C.; Uhlarz, M.; Hayden, S. M.; Vollmer, R.; Löhneysen, H. V.; Bernhoeft, N. R.; Lonzarich, G. G. *Nature* **2001**, *412*, 58.
(112) Bernhard, C.; Tallon, J. L.; Niedermayer, C.; Blasius, T.; Golnik, A.; Brücher, E.; Kremer, K.; Noakes, D. R.; Stronach, C. E.; Ansaldo, E. J. *Phys. Rev*. **1999**, *B 59*, 14099.

CR030657D